arXiv:2206.03449v3 [math.NA] 11 Jan 2024

The virtual element method on polygonal pixel–based tessellations*

S. Bertoluzza[a], M. Montardini[b,a], M. Pennacchio[a], D. Prada[a,]

[a]*IMATI "E. Magenes", CNR, via Ferrata, 5A, Pavia, 27100, PV, Italy*
[b]*Dipartimento di Matematica, Universita di Pavia, via Ferrata, 5, Pavia, 27100, PV, Italy*

Abstract

We analyze and validate the virtual element method combined with a boundary correction similar to the one in [1, 2], to solve problems on two dimensional domains with curved boundaries approximated by polygonal domains obtained as the union of squared elements out of a uniform structured mesh, such as the one that naturally arises when the domain is issued from an image. We show, both theoretically and numerically, that resorting to the use of polygonal elements allows to satisfy, for any order, the assumptions required for the stability of the method, thus allowing to fully exploit the potential of higher order methods, the efficiency of which is ensured by a novel static condensation strategy acting on the edges of the decomposition.

Keywords: Virtual element method, polygonal approximating domain, smooth boundary, curved boundary

1. Introduction

The simplest (and cheapest!) meshes that can be used to approximate a complex domain are the ones whose elements coincide with elements of a sufficiently fine squared/cubic uniform structured grid. This holds particularly true when the

*This paper has been realized in the framework of the ERC Project CHANGE, under the EU's Horizon 2020 programme (grant agreement No 694515). It was co-funded by the MIUR Progetti di Ricerca di Rilevante Interesse Nazionale (PRIN) Bando 2017 (grant 201744KLJL) and Bando 2020 (grant 20204LN5N5). M. Pennacchio has been partially supported by ICSC—Centro Nazionale di Ricerca in High Performance Computing, Big Data, and Quantum Computing funded by European Union—NextGenerationEU. The authors are members of INDAM-GNCS.

Email addresses: silvia.bertoluzza@cnr.it (S. Bertoluzza), monica.montardini@unipv.it (M. Montardini), micol.pennacchio@imati.cnr.it (M. Pennacchio), daniele.prada@imati.cnr.it (D. Prada)

January 12, 2024

domain is retrieved from the results of some imaging procedure, as it often happens, for instance, in medical applications. In such a framework (an approximation of) the physical domain is already given as the union of pixels/voxels, that can be seen as elements of a very fine structured quadrangular/hexahedral mesh. The polygonal/polyhedral domain obtained as the union of the pixels/voxels that a segmentation procedure tags as belonging to the physical object of interest, can then be used as an approximation of the physical domain, to be used in the numerical solution of a PDE, modeling some physical behavior.

It is a well known fact that approximating the solution of a problem in a physical domain by simply solving, by a finite element method, a problem in an approximated polygonal domain, with a boundary condition somehow "copied" from the physical boundary data, yields, for methods of higher order, a suboptimal result. For homogeneous Dirichlet boundary value problems, the fact itself of approximating the physical domain (with curved boundary) introduces an error that, even in the best of cases, can be of the order $\delta^{3/2}$, δ being the distance between physical and approximate boundary [3]. This leads to suboptimality whenever the order k of the method is greater than two. In the framework we are considering the situation is worse, and the method turns out to be suboptimal also for $k = 1$, with a convergence of order only $h^{1/2}$, h denoting the meshsize, as observed, both theoretically and numerically, in [4]. Nevertheless, such an approach is currently used by many practitioners, that, resorting to a so called *microFEM* approach ([5]), use the mesh whose elements coincide with the voxels in a microCT scan, in order to simulate some physical phenomenon taking place in an underlying (unknown) domain. Of course, given the extreme fineness of the mesh, the results obtained by such an approach turn out to be sufficiently accurate, but with a cost that is much higher, when compared to the cost of the finite element method of the same accuracy on polygonal physical domains.

Different options exist to counter the sources of error related to the approximation of the domain, and thus obtain a more efficient method, provided, of course, we can rely on information on the actual physical domain, that needs to be retrieved and somehow, leveraged. By what means, and how accurately, such information can be retrieved from available imaging data is a crucial question that is, however, out of the scope of this paper (we refer to [6] and the references therein for an up to date survey on edge detection methods that can be used to this aim). Once this information is available, one option is to work on a possibly coarser mesh (remark that preprocessing the image by changing its resolution is an easy way to obtain a coarser versions of the domain approximation), and either use a fictitious domain approach, as in the finite cell method [7], or state the problem on the actual domain by "cutting" the elements

that cross the boundary, as done in the cutFEM method [8]. These approaches can also be combined with different discretization methodologies such as isogeometric analysis [9].

A different approach consists in resorting, while working on the approximate domain, to techniques specifically designed to take into account the fact that its boundary does not coincide with the actual curve/surface where boundary conditions should be prescribed. The first example of this strategy was introduced already in the early '70s in the seminal paper by Bramble, Dupont and Thomée [10]. There, for convex domains in 2D, a Taylor extrapolation along the direction normal to the boundary of the approximating polygonal domain was leveraged, within a Nitsche approach, to weakly impose the correct boundary conditions. Introduced in the late 2010s, and already tested in different application fields (see, e.g., [11, 12, 13, 14]), the *shifted boundary method* (SBM, see [15, 16]) overcomes many of the limitations of the original Bramble, Dupont and Thomée approach (BDT), by a careful choice of the extrapolation direction and a clever design of the stabilization term for the underlying Nitsche method. Initially limited to order up to two, an high order version of the SBM has been recently introduced and analyzed in [1], allowing, in principle, to attain any arbitrary order k. In [17] a variant of the BDT method is proposed, based on the Lagrange multiplier method for Dirichlet boundary conditions [18], for which, in the spirit of [19], the relation with Nitsche's method with boundary correction is also discussed. The latter is also studied in the framework of the cutFEM method in [20], where the analysis is carried out for an a priori arbitrary choice of the extrapolation direction, which is then, in practice, chosen to be, as in SBM, normal to the boundary of the physical domain. The *polynomial extension finite element method* ([21]) avoids the problem of choosing an extrapolation direction by replacing Taylor extrapolation with an *averaged Taylor polynomial extrapolation* to also attain arbitrary order under suitable conditions. Similar ideas can be also leveraged in the discontinuous Galerkin framework ([22]).

Unfortunately, as the order k of the method gets higher, the approximate domains that we are considering eventually fail, when discretized by finite elements, to satisfy one of the assumptions required for the stability of such methods, namely that the ratio between the distance from the approximate to the true boundary and the diameter of the elements is lower than a constant that decreases to zero as k increases. A way to overcome this limitation is to replace the fine mesh with a sufficiently coarser polygonal/polyhedral mesh, obtained by agglomeration, thus making the diameter of the elements larger, while keeping the distance of the two boundaries fixed. On the new polygonal/polyhedral mesh, one can then combine a boundary correction strategy with one of the discretization methods capable of handling polytopal meshes.

In this direction, in [23] the authors combine a polynomial extension method with a *weak Galerkin* finite element method, while in [24, 2] a boundary correction method similar to the one in [20] is combined with *virtual elements* (VEM, [25, 26, 27]), a methodology that, thanks to its flexibility, its robustness (in particular with respect to the shape of the elements), and its potential for high accuracy (the discretization can be designed to be of arbitrarily high order, [28]), has, since its introduction in the early 2010's, rapidly gathered the attention of the scientific community, resulting in extensions to deal with different type of equations ([29, 30, 31, 32, 33, 34, 35, 36, 37, 38, 39, 40, 41, 42, 43]), different formulations ([44, 45, 46, 47, 48]) and numerous applications ([49, 50, 51, 42, 52, 53]).

The aim of this paper is to propose and validate, initially in two dimensions, the use of the combination of virtual elements and boundary correction methods such as BDT or SBM, as a way to obtain an efficient solver in the context presented previously. To this aim we will need to adapt the theoretical results obtained in [2] to the present framework. Indeed, tessellations whose elements are obtained as the union of squares of a structured uniform mesh, do not satisfy the standard shape regularity assumptions under which virtual element methods are usually analyzed. We will also need to show how to efficiently handle elements with a large number of small edges, deriving from the agglomeration process.

The paper is organized as follows. In Section 2 we introduce a unified notation for a class of boundary correction methods that includes, among others, the BDT method and some of its variants, as well as the high order SBM. In Section 3 we recall definition and properties of the plain virtual element method, and we present the virtual element method for curved domains [2] obtained by combining the VEM with the previously introduced boundary correction methods. In Section 4 we present a static condensation procedure allowing to keep the resulting linear system small, also in the presence of elements with a large number of small edges. In Section 5 we present the numerical results attesting to the validity of our proposal and comparing the performance attainable with virtual elements with those obtained by the same boundary correction approach in the finite element framework. The proofs of several theoretical bounds and estimates, needed to extend known virtual element results to the present framework, are presented in three appendixes.

2. Boundary correction methods in the finite element framework

For the sake of simplicity, we focus on a simple model problem, namely on the Poisson equation

$$-\Delta u = f, \text{ in } \Omega, \qquad u = g \text{ on } \Gamma = \partial\Omega, \tag{1}$$

where $f \in L^2(\Omega)$, $g \in H^{1/2}(\partial\Omega)$, and where $\Omega \subseteq \mathbb{R}^2$ is a convex domain with a curved boundary $\Gamma = \partial\Omega$, assumed, for the sake of convenience, to be of class C^∞. We consider here a context where the domain is not directly available but is obtained as the result of an imaging process. We will then only have an approximation of Ω, which we will denote by Ω_h, naturally decomposed as the union of (tiny) squared elements (the pixels) of size $h \times h$, with edges parallel to the axes. We will not address here the segmentation problem that needs to be solved in order to single the approximated domain Ω_h out of the image. It is natural, in this context, to assume that for all $\mathbf{x} \in \partial\Omega_h$, the distance $\mathrm{d}(\mathbf{x}, \partial\Omega)$ of $\mathbf{x}$ to $\partial\Omega$ verifies $\mathrm{d}(\mathbf{x}, \partial\Omega) \lesssim h$ (this is another way to say that Ω_h is an approximation to Ω). This happens for instance if Ω_h is constructed by retaining all the squares contained in Ω.

The simplest method to solve (1) (and one of the most used by practitioners) is the finite element method on the quadrilateral mesh $\mathcal{T}_h$, whose elements are the pixels, in which Ω_h is naturally split. The approximate solution is looked for in the standard Q_k finite element space

$$V_h = \{v \in C^0(\Omega_h) : \ v|_K \in \mathbb{Q}_k \ \forall K \in \mathcal{T}_h\},$$

($\mathbb{Q}_k$ denoting the space of polynomials $p(x, y)$ of degree at most k both in x and in y) and, using Nitsche's method (see [54]) to impose the boundary conditions, it is defined as the element $u_h \in V_h$ such that for all $v \in V_h$ it holds

$$\int_{\Omega_h} \nabla u_h \cdot \nabla v - \int_{\partial\Omega_h} \partial_{\nu_h} u_h \, v - \int_{\partial\Omega_h} u_h \left(\partial_{\nu_h} v - \gamma h^{-1} v\right) = \int_{\Omega_h} f v - \int_{\partial\Omega_h} g^\star (\partial_{\nu_h} v - \gamma h^{-1} v), \quad (2)$$

with $g^\star$ suitably defined, where ν_h is the outer unit normal to $\partial\Omega_h$, $\gamma > 0$ is a suitable, sufficiently large, scalar constant, and where $\partial_{\nu_h} v \in L^2(\partial\Omega_h)$ denotes the $L^2(\partial\Omega_h)$ function coinciding with $\nabla u_h \cdot \nu_h$ on each boundary edge of the mesh $\mathcal{T}_h$. It is however known that, in our framework, such a method is suboptimal already for $k = 1$ (see [4]), and several strategies have been proposed in order to retrieve the optimal order of approximation for the finite element solution on approximating polygonal domains, relying on the idea of suitably correcting the Nitsche's formulation (2) so that the boundary condition is somehow imposed on the original boundary, while still maintaining all computations on the approximating domain.

We consider here a general formulation that encompasses a number of such strategies. We let $\mathcal{E}^\partial$ denote the set of edges of $\mathcal{T}_h$ lying on $\partial\Omega_h$, and, for $\mathbf{x} \in \partial\Omega_h$, we

let $\sigma(\mathbf{x})$ denote an outward unit vector. Assuming that $\Omega_h \subseteq \Omega$, for $\mathbf{x} \in \partial\Omega_h$ we let $\delta(\mathbf{x}) > 0$ denote the distance to $\partial\Omega$ along the direction σ, that is, the smallest non negative scalar such that

$$\mathbf{x} + \delta(\mathbf{x})\sigma(\mathbf{x}) \in \partial\Omega.$$

Letting $\partial_\sigma^j u = (\partial_\sigma)^j u$ denote the $L^2(\partial\Omega_h)$ function coinciding, on each edge. with the j-th partial derivative of u in the σ direction, and letting, for $\mathbf{x} \in \partial\Omega_h$, $g^\star(\mathbf{x})$ be defined as

$$g^\star(\mathbf{x}) = g(\mathbf{x} + \delta(\mathbf{x})\sigma(\mathbf{x})),$$

we look for $u_h \in V_h$ such that for all $v \in V_h$ it holds that

$$\begin{aligned}\int_{\Omega_h} \nabla u_h \cdot \nabla v - \int_{\partial\Omega_h} \partial_{\nu_h} u_h v - \sum_{e\in\mathcal{E}^\partial} \int_e (u_h + \mathscr{C}[u_h]) \left(\partial_{\nu_h} v - \gamma h^{-1}(v + \widehat{\mathscr{C}}[v])\right) \\ = \int_{\Omega_h} fv - \sum_{e\in\mathcal{E}^\partial} \int_e g^\star \left(\partial_{\nu_h} v - \gamma h^{-1}(v + \widehat{\mathscr{C}}[v])\right), \quad (3)\end{aligned}$$

where the "correction" term for the trial and test functions are defined as

$$\mathscr{C}[w] = \sum_{j=1}^{k} \frac{\delta^j}{j!} \partial_\sigma^j w, \qquad \widehat{\mathscr{C}}[w] = \sum_{j=1}^{\widehat{k}} \frac{\delta^j}{j!} \partial_\sigma^j w. \quad (4)$$

Different choices have been proposed in the literature for the extrapolation direction σ and for the parameter $\widehat{k}$ involved in the definition of $\widehat{\mathscr{C}}[\cdot]$ in (4), resulting in different correction methods. The choice $\widehat{k} = 0$ (which is to be interpreted as $\widehat{\mathscr{C}}[v] = 0$) and $\sigma = \nu_h$ yields the method originally proposed in the seminal work [10] by Bramble, Dupont and Thomée. Choosing $\widehat{k} = 1$ and $\sigma(\mathbf{x}) = \nabla \mathrm{d}(\mathbf{x}, \partial\Omega) = \nu^\star$, (that is $\sigma(\mathbf{x}) = \nu(\mathbf{x}+\delta(\mathbf{x})\sigma(\mathbf{x}))$, ν denoting the outer unit normal to $\partial\Omega$) yields the high order shifted boundary method (SBM) proposed in [1]. The choice $\widehat{k} = 0$ and σ a priori arbitrary is analyzed in [8] and in [54, 24], where it is respectively exploited in the context of the cut finite element method, and in the virtual element framework. In both cases σ is in practice also chosen as the gradient of the distance function to the boundary, so that $\delta(\mathbf{x})$ is as small as possible.

For all these choices it is possible to prove that, under the condition that $\delta_h = \max_{x\in\partial\Omega_h} |\delta(x)| < \tau h$, with $\tau > 0$ a constant depending on the order k, and provided γ is large enough, the method is stable, and converges with optimal order. The (small) constant τ decreases to 0 as k increases. If the domains are constructed in such a way that $\delta_h = o(h)$, for all these choices and for all order k there exists a

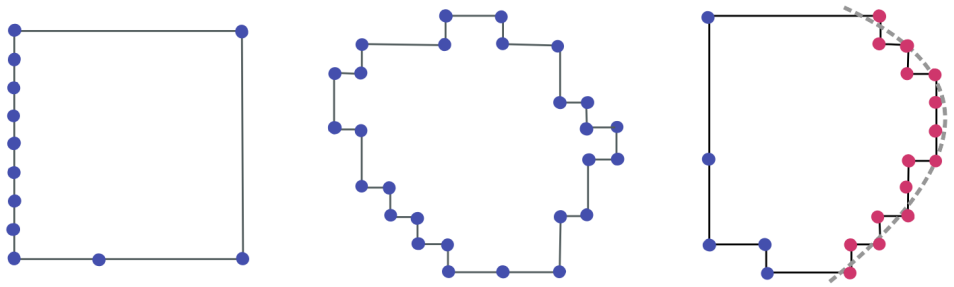


Figure 1: Three possible elements of the tessellation $\mathcal{T}_H$. For the sake of the exposition, boundary edges (with vertices marked in red) are never agglomerated to form larger edges, even when this is possible. Agglomeration of interior edges (vertices in blue) into larger edges fits instead in our exposition.

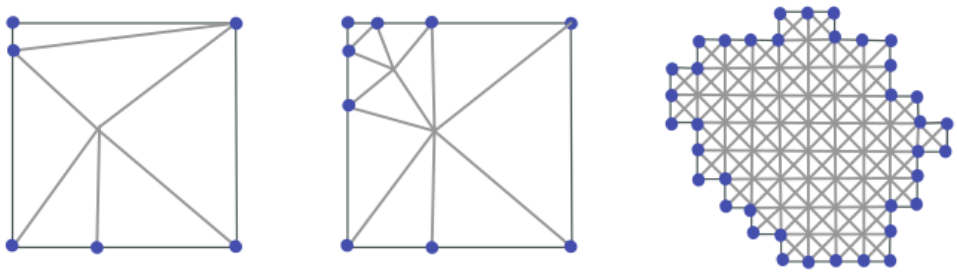


Figure 2: Three examples of the auxiliary triangulation $\widetilde{\mathcal{T}}_K$. As one can see in the leftmost example, the presence of two adjacent boundary edges with very different length results in a badly shaped triangle. Adding few nodes, as in the central example, may improve the shape regularity of the triangulation. As the $\widetilde{\mathcal{T}}_K$ is allowed to have a number of elements as large as needed, the presence of a large number of very small edges does not, in itself, result in badly shaped triangulation (see the rightmost example).

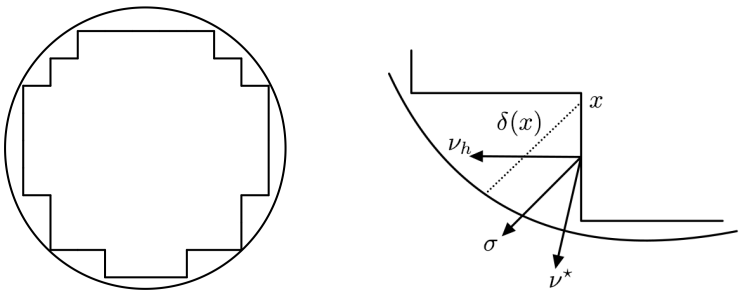


Figure 3: An approximate domains Ω_h falling in our framework. The theoretical framework does not in principle require the extrapolation direction σ to coincide with either the normal ν_h to the approximate boundary or the normal $\nu^\star$ to the physical boundary, though the latter is generally the best choice.

h_0 such that, provided γ is large enough, for all $h < h_0$ the method is stable and converges with optimal order.

Unfortunately the class of polygons that we are considering in our framework does not satisfy the condition that $\delta_h = o(h)$. Indeed, in general, for approximating domains issued from imaging, which are the union of equal square elements (pixels), we have that[1] $\delta_h \simeq h$. Consequently, there exist a $\bar{k}$ such that for $k > \bar{k}$ our tessellations will not satisfy the condition $\delta_h \leqslant \tau h$, and, as k increases all the considered methods will eventually lose stability.

Remark 2.1. Other boundary correction strategies can be found in the literature that we could include in the unified formulation (3), provided we allow more general forms for the correction terms $\mathscr{C}$ and $\widehat{\mathscr{C}}$, than the ones in (4). We recall the polynomial extension method ([21], see also [22]).

3. The Virtual Element Discretization

The main idea behind the method we are proposing is to discretize the polygonal approximate domain Ω_h with a polygonal tessellation $\mathcal{T}_H$, with meshsize H, whose elements are obtained as union of quadrilateral elements of the fine tessellation $\mathcal{T}_h$. On the tessellation $\mathcal{T}_H$ we can then use the virtual element Nitsche's method with boundary correction proposed in [24, 2]. By taking particular care in the implementation, this will result in a method with a much more favorable cost/performance ratio than the one obtained by plain finite elements as used in the microFEM approach, without the need for modifying the bulk bilinear form near the boundary. To this aim, we start by reviewing the definition of the method we will be employing, as proposed in [2].

3.1. The tessellation

We assume that the tessellation $\mathcal{T}_H$ of Ω_h into polygons, obtained by agglomeration of the square elements of $\mathcal{T}_h$, satisfies the following Assumption.

[1] Unless the specific value of the constant C is explicitely needed, throughout the paper we will write $A \lesssim B$ (resp. $A \gtrsim B$) to indicate that the quantity A is bounded from above (resp. from below) by a constant C times the quantity B, with C possibly depending on Ω as well as on the parameters α_0 and N_0 appearing in the shape regularity assumption 3.1, but otherwise independent of the shape and size of the elements of the tessellations. The notation $A \simeq B$ will stand for $A \lesssim B \lesssim A$.

Assumption 3.1. All elements $K \in \mathcal{T}_H$ are simply connected union of squares of the cartesian mesh $\mathcal{T}_h$ of meshsize h. Moreover, letting for $K \in \mathcal{T}_H$

$$H_K = \max_{(x,y),(x',y') \in \mathcal{T}_H} \max\{|x - x'|, |y - y'|\},$$

we have $H_K \simeq H$ and there exists constants α_0, N_0 such that:

(i) each element $K \in \mathcal{T}_H$ verifies $S(\mathbf{x}_K, \alpha_0 H_K) \subset K \subset S(\mathbf{x}_K, H_K)$, $\mathbf{x}_K = (x_K, y_K)$ denoting the geometrical center of K and $S(\mathbf{x}_K, d)$ the square of center $\mathbf{x}_K$ and side d;

(ii) for all $x \in (x_K - H_K/2, x_K + H_K/2)$ (resp. $y \in (y_K - H_K/2, y_K + H_K/2)$) there exist at most N_0 values $y \in \mathbb{R}$ (resp. $x \in \mathbb{R}$) such that $(x, y) \in \partial K_{\text{hor}}$ (resp. $(x, y) \in \partial K_{\text{ver}}$), ∂K_{hor} and ∂K_{ver} respectively denoting the union of horizontal and vertical edges of K.

In order to prove the virtual element approximation estimate, we will also need to make the following additional assumption, where the shape regularity constant of a triangulation is intended as the maximum over all triangles T of the ratio h_T/ρ_T, h_T and ρ_T respectively denoting the diameter of the circumscribed and inscribed circle.

Assumption 3.2. There exists a constant α_1 such that for each element $K \in \mathcal{T}_H$ there exists a conforming triangulation $\widetilde{\mathcal{T}}_K$ of K with shape regularity constant at most α_1, whose set of boundary edges coincides with the set of edges of K.

In the above assumption we do not require the number of elements of $\widetilde{\mathcal{T}}_K$ to be uniformly bounded. We underline that the triangulation $\widetilde{\mathcal{T}}_K$ only plays a role in the theoretical analysis of the method, and its actual construction is not needed for the design and implementation of the method.

Remark 3.3. In the present framework, it is always possible to build a triangulation $\widetilde{\mathcal{T}}_K$ of K, whose set of boundary edges coincides with $\mathcal{E}^K$. In general, however, we can only guarantee that for T in $\widetilde{\mathcal{T}}_K$, $h_T/\rho_T \lesssim H/h$. Remark that the presence of very small edges is not problematic in itself, but, as illustrated in figure 2, the bad situations are rather the ones where very small edges are adjacent to large edges.

Assumption 3.1 is not sufficient to imply the validity of the standard shape regularity assumption on which the analysis of the virtual element method relies. In particular, it does not imply star shapedness of the element with respect to all points in a ball of radius of order H. We can however show that it is sufficient to obtain a

number of bounds which are usually proven under more restrictive assumptions. In particular, the following bounds, which we prove in Appendix A, hold with constants only depending on α_0, α_1 and N_0.

Lemma 3.4. *Under Assumption 3.1, for all $\varphi \in H^1(K)$ it holds that*

$$\|\varphi\|_{0,\partial K} \lesssim H^{-1/2}\|\varphi\|_{0,K} + H^{1/2}|\varphi|_{1,K}. \tag{5}$$

Additionally, for all $p \in \mathbb{P}_k$ we have that

$$\|p\|_{0,\partial K} \lesssim H^{-1/2}\|p\|_{0,K}. \tag{6}$$

Moreover, provided Assumption 3.2 also holds, for all $v \in H^r(K)$, $r \geqslant 1$, we have that

$$\sum_{e\in\mathcal{E}^K} |v|^2_{r-1/2,e} \lesssim |v|^2_{r,K}, \tag{7}$$

where $\mathcal{E}^K$ denotes the set of edges of the polygon K.

For the sake of notational simplicity we also make the minor assumption that the set of boundary edges of $\mathcal{T}_H$ coincides with $\mathcal{E}^\partial$, which, we recall, is the set of boundary edges of the fine mesh $\mathcal{T}_h$, that is, all boundary nodes of $\mathcal{T}_h$ are also boundary nodes of $\mathcal{T}_H$ (see Figure 1). Remark however that all the result presented here carry over to the case where we allow also the boundary edges of $\mathcal{T}_H$ to be agglomerations of boundary edges of $\mathcal{T}_h$.

3.2. The virtual element space

We will consider the standard order $k \geqslant 2$ enhanced virtual element discretization space [25], whose definition we briefly recall. For each polygon $K \in \mathcal{T}_H$ we let the space $\mathbb{B}_k(\partial K)$ be defined as

$$\mathbb{B}_k(\partial K) = \{v \in C^0(\partial K) : v|_e \in \mathbb{P}_k \ \forall e \in \mathcal{E}^K\},$$

where, we recall, $\mathcal{E}^K$ denotes the set of edges of the polygon K. A local space $\widetilde{V}^{K,k}$ is defined as

$$\widetilde{V}^{K,k} = \{v \in H^1(K) : \ v|_{\partial K} \in \mathbb{B}_k(\partial K), \ \Delta v \in \mathbb{P}_k\},$$

and we introduce the operator $\Pi_K^{\nabla,k} : H^1(K) \to \mathbb{P}_k$ defined as

$$\int_K \nabla\Pi_K^{\nabla,k} v \cdot \nabla q = \int_K \nabla v \cdot \nabla q, \quad \forall q \in \mathbb{P}_k, \qquad \int_K \Pi_K^{\nabla,k} v = \int_K v.$$

The local VE space is then defined ([27]) as

$$V^{K,k} = \{v \in \widetilde{V}^{K,k} : \int_K vq = \int_K \Pi_K^{\nabla,k} vq, \ \forall q \in \mathbb{P}_k \cap \mathbb{P}_{k-2}^{\perp}\},$$

where $\mathbb{P}_k \cap \mathbb{P}_{k-2}^{\perp}$ denotes the $L^2(K)$ orthogonal complement of $\mathbb{P}_{k-2}$ in $\mathbb{P}_k$. The global discrete VE space V_H is finally obtained by glueing the local spaces continuously:

$$V_H = \{v \in H^1(\Omega) : v|_K \in V^{K,k} \ \forall K \in \mathcal{T}_H\}. \tag{8}$$

A function in V_H is uniquely determined by the following degrees of freedom

- its values at the vertices of the tessellation;
- for each edge e, its values at the $k-1$ internal points of the $k+1$-points Gauss-Lobatto quadrature rule on e;
- for each element K, its moments in K up to order $k-2$.

The following lemma, usually proven under stronger shape regularity assumptions, also holds under Assumption 3.1, as we show in Appendix B.

Lemma 3.5. *For any given function $u \in H^2(\Omega)$ we can define a unique function $u_I \in V_H$ such that, if $u \in H^s(K)$ with $2 \leqslant s \leqslant k+1$ we have*

$$|u - u_I|_{1,K} \lesssim H_K^{s-1} |u|_{s,K}. \tag{9}$$

We recall now that a key concept in the definition of virtual element methods is the one of *computability*. Essentially, operators or bilinear forms, acting on virtual element functions, are said to be computable if the knowledge of the degrees of freedom of the argument functions is sufficient for the direct evaluation of the operator/bilinear form, without the need of solving the PDEs implicitly involved in the definition of $V^{K,k}$. The elliptic projector $\Pi_K^{\nabla,k} : V^{K,k} \to \mathbb{P}_k$ is computable [25], while the bilinear form $a : V_H \times V_H \to \mathbb{R}$ and its local counterpart $a^K : V^{K,k} \times V^{K,k} \to \mathbb{R}$

$$a(\varphi, \psi) = \int_\Omega \nabla\varphi \cdot \nabla\psi, \qquad a^K(\varphi, \psi) = \int_K \nabla\varphi \cdot \nabla\psi,$$

are not. In the definition of the virtual element discretization, the bilinear form a is replaced by a computable approximate bilinear form $a_H : V_H \times V_H \to \mathbb{R}$

$$a_H(\varphi, \psi) = \sum_K a_H^K(\varphi, \psi),$$

where the elemental approximate bilinear form $a_H^K : V^{K,k} \times V^{K,k} \to \mathbb{R}$ is defined as

$$a_H(\varphi, \psi) = a^K(\Pi_K^{\nabla,k}(\varphi), \Pi_K^{\nabla,k}(\psi)) + \beta S_a^K(\varphi - \Pi_K^{\nabla,k}(\varphi), \psi - \Pi_K^{\nabla,k}(\psi)),$$

$\beta > 0$ being a constant parameter to be chosen later, and the stabilizing bilinear form S_a^K being any computable symmetric bilinear form satisfying

$$c_* a^K(\varphi, \varphi) \leqslant S_a^K(\varphi, \varphi) \leqslant C^* a^K(\varphi, \varphi), \quad \forall \varphi \in V^{K,k} \text{ with } \Pi^\nabla \varphi = 0, \tag{10}$$

with c_* and C^* two positive constants independent of K. Different choices for the bilinear form S_a^K are available in the literature (see [55]), several of which reduce, when expressed in terms of the degrees of freedom, to a suitably scaled euclidean scalar product [28].

Letting $H^1(\mathcal{T}_H)$ and $\mathbb{P}_k(\mathcal{T}_H)$ respectively denote the spaces of discontinuous piecewise H^1 functions and of discontinuous piecewise polynomials of order up to k, defined on the tessellation $\mathcal{T}_H$:

$$H^1(\mathcal{T}_H) = \{v \in L^2(\Omega_h) : \ v|_K \in H^1(K) \text{ for all } K \in \mathcal{T}_H\},$$
$$\mathbb{P}_k(\mathcal{T}_H) = \{v \in L^2(\Omega_h) : \ v|_K \in \mathbb{P}_k(K) \text{ for all } K \in \mathcal{T}_H\},$$

it will be convenient in the following to introduce the global projector $\Pi^\nabla : H^1(\mathcal{T}_H) \to \mathbb{P}_k(\mathcal{T}_H)$ defined by $\Pi^\nabla(v)|_K = \Pi_K^{\nabla,k}(v|_K)$ for all $K \in \mathcal{T}_H$. Moreover, we let $\Pi^0 : L^2(\Omega_h) \to \mathbb{P}_k(\mathcal{T}_H)$ denote the $L^2(\Omega_h)$ orthogonal projection onto the space of discontinuous piecewise polynomials of degree at most k.

3.3. Nitsche's method with boundary correction for VEM

In order to discretize Problem (1) we substantially follow [2], with some minor differences that will allow to make the method more efficient (see Remark 4.1). More precisely, we assume that $\Omega_h \subseteq \Omega$ and we choose, on $\partial\Omega_h$, an outward direction σ, not necessarily normal to $\partial\Omega$ or $\partial\Omega_h$, which we assume to be constant on each edge e (see Figure 3). For $u \in L^2(\Omega_h)$ with $u \in C^m(\bar{K})$ for all $K \in \mathcal{T}_H$, we let $\partial_\sigma^m u$ denote the $L^2(\partial\Omega_h)$ function coinciding, on each boundary edge of $\mathcal{T}_H$, with the m-th derivative of u in the direction σ. We recall that for $x \in \partial\Omega_h$, $\delta(x) > 0$ denotes the smallest non negative scalar such that

$$\mathbf{x} + \delta(\mathbf{x})\sigma(\mathbf{x}) \in \partial\Omega.$$

We look for $u_h \in V_H$ such that for all $v \in V_H$ it holds that

$$
\begin{aligned}
a_H(u_h, v) - \int_{\partial\Omega_h} \partial_\nu \Pi^\nabla(u_h) v \\
- \int_{\partial\Omega_h} \left(\Pi^\nabla(u_h) + \mathscr{C}\left[\Pi^\nabla(u_h)\right]\right) \left(\partial_{\nu_h} \Pi^\nabla(v) - \gamma H^{-1}(\Pi^\nabla(v) + \widehat{\mathscr{C}}\left[\Pi^\nabla(v)\right])\right) \\
= \int_{\Omega_h} f\Pi^0(v) - \int_{\partial\Omega_h} g^\star \left(\partial_{\nu_h} \Pi^\nabla(v) - \gamma H^{-1}(\Pi^\nabla(v) + \widehat{\mathscr{C}}\left[\Pi^\nabla(v)\right])\right) \quad (11)
\end{aligned}
$$

with $g^\star(\mathbf{x}) = g(\mathbf{x} + \delta(\mathbf{x})\sigma)$, and with $\mathscr{C}[w]$ and $\widehat{\mathscr{C}}[w]$ defined in (4).

The analysis of equation (11) relies on the assumption that the discrete boundary $\partial\Omega_h$ is sufficiently close to the true boundary $\partial\Omega$. More precisely, in order for (11) to be well posed and yield an optimal error estimate, we need to assume that for some constant $\tau \in (0, 1)$, sufficiently small, we have that

$$
\max_{K\in\mathcal{T}_H} \max_{\mathbf{x}\in\partial K\cap\partial\Omega_h} \frac{\delta(\mathbf{x})}{H} \leqslant \tau. \quad (12)
$$

When Ω_h is constructed as the union of all elements in the fine mesh $\mathcal{T}_h$ wich are included in Ω, such assumption reduces to

$$
\widehat{\tau} := \frac{h}{H} \leqslant C\tau,
$$

the constant C being the constant such that $\delta/H_K \leqslant Ch/H$. If such an assumption is satisfied, existence and uniqueness of the solution of (11) can be proven by an identical argument to the one in [24, 2], which also yields an error estimate (see [2]) in the norm $|||\cdot|||_{\Omega_h}$, defined as

$$
|||\varphi|||^2_{\Omega_h} = |\Pi^\nabla\varphi|^2_{1,\mathcal{T}_H} + |\varphi - \Pi^\nabla\varphi|^2_{1,\mathcal{T}_H} + H^{-1}\|\Pi^\nabla\varphi + \widehat{\mathscr{C}}\left[\Pi^\nabla\varphi\right]\|^2_{0,\partial\Omega_h},
$$

where we set $|\varphi|^2_{1,\mathcal{T}_H} = \sum_{K\in\mathcal{T}_H} |\varphi|^2_{1,K}$. More precisely, we have the following theorem.

Theorem 3.6. *There exists $\beta_0 > 0$ and $\gamma_0 > 0$ such that, provided $\beta > \beta_0$, for all $\gamma > \gamma_0$, the following holds: there exists a constant τ_γ, depending on γ, such that if* (12) *holds for $\tau < \tau_\gamma$, Problem* (11) *is well posed, and, if $u \in H^{k+1}(\Omega) \cap W^{m,\infty}(\Omega)$, $m \leqslant k + 1$ we have the following error bound:*

$$
|||u - u_h|||_{1,\Omega_h} \lesssim H^k |u|_{k+1,\Omega} + H^{-1/2} h^m |u|_{m,\infty,\Omega}.
$$

Observe that as $\Pi^\nabla + \widehat{\mathscr{C}} \circ \Pi^\nabla$ preserves the constants, $|||\cdot|||_{1,\Omega_h}$ is indeed a norm on $H^1(\Omega_h)$. Theorem 3.6 has been proven in [24] for the case $\widehat{k} = 0$ with a slightly

different formulation of equation (11). The proof for the new, more general, formulation is fundamentally the same, but, for the sake of completeness we report it in Appendix C.

Remark 3.7. We point out that, as γ_0 is independent of the parameter c_* appearing in the condition (10) on the stabilization bilinear form S_a^K, the parameter γ in (11) can be chosen independently of the choice of S_a^K.

Remark 3.8. By assuming Ω to be of class C^∞, and allowing σ to be an arbitrary direction, we somehow seem to avoid the problems related with the choice of the extrapolation direction (particularly in the vicinity of the singular points of Ω). In particular, Theorem 3.6 is valid for any choice of σ. Of course, is σ is badly chosen, the conditions on δ required by such theorem for stability will be more difficult to satisfy. The actual choice of σ will be guided both by the result of Theorem 3.6 (in particular, by the condition $\tau < \tau_\gamma$ that suggests that σ be chosen so that δ is as small as possible), and by practical considerations related to the numerical evaluation of the edge integrals in the bilinear form (3), which suggest to choose σ so that $\sigma|_e$ is smooth for all edges even in the presence of corners in the physical domain. In this last case, we refer to [56] for a strategy for the choice of the extrapolation direction.

Remark 3.9. We want to recall here that other approaches exist to adapting the VEM to deal with curved boundaries in 2D. Both [57] and [58] propose versions of the VEM that handle elements with curved edges, which can be fitted to the actual physical boundary. Several extensions and applications are found in [59, 60, 61, 62]. As always, there are advantages and disadvantages in both approaches. In particular, while the use of elements with curved edges also allows to deal with curved interfaces, which we do not presently treat, the boundary correction approach has the main advantage that, in a geometry adaptive procedure where the knowledge of the actual physical boundary (implicitely defined by the image) is iteratively improved, modifications of the boundary only imply the modification of the correction term, with no need of recomputing the bulk integrals in the boundary adjacent elements.

4. Static condensation of the "lazy" degrees of freedom

While, depending on the ratio H/h, the number of degrees of freedom for the VE space V_H can be much lower than the one for the finite element space V_h, it might still be quite high and, more importantly, the discretization (11) leads to a linear system with a matrix that may have some large dense blocks. This happens whenever an element K presents a large number of small edges, which, in our framework, always happens at least for boundary elements. While in 2D this does not yet pose a major problem, in order for our approach to be viable also in 3D, we need to tackle this

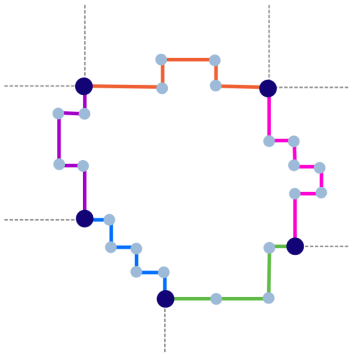


Figure 4: One element with 27 edges and 5 macro edges.

issue. In order to do so, we start with the observation that the bilinear form on the left hand side of (11) can be split into two components: a consistency component that only sees the test and trial functions after the action of the operator Π^∇, and a stability component, only needed for ensuring the well posedness of the discrete equation. The consistency component has, in our framework, a large kernel, whose elements are only seen by the stability part of the bilinear form. In principle, we could then factor out such a kernel and restrict the discrete problem to a smaller space without losing the approximation properties. Unfortunately, the splitting of V_H into $\ker(\Pi^\nabla) \oplus \mathring{V}_H$ (with $\mathring{V}_H \subset V_H$ being a complement, not necessarily orthogonal, of $\ker(\Pi^\nabla)$ into V_H) is, a priori, a non local operation that would require a singular value decomposition of a large matrix, so that a full computation of such a splitting is not a viable option. We can however single out blocks of degrees of freedom on which such an operation can be performed locally. To do so, we start by introducing the macro edges of the tessellation, where a macro edge E is either a maximal connected component of $\partial K \cap \partial K'$, or a maximal connected component of $\partial K \cap \partial \Omega_h$, with $K, K' \in \mathcal{T}_H$ (see Figure 4). We observe that, in our framework, it generally happens that, at least macro edges on the boundary, but possibly also interior macro edges, are the union of a significant number of edges of the tessellation.

Let then E be a macro edge, and consider the subset $V_E \subset V_H$ defined as

$$V_E = \{v \in V_H : v = 0 \ \text{ on } \ \cup_K \partial K \backslash E, \ \int_K vp = 0, \ \forall K \in \mathcal{T}_H, \ p \in \mathbb{P}_{k-2}\}.$$

We easily see that, for a non zero $v \in V_E$, $v|_K \neq 0$ if and only if E is a macro edge of K. For $v \in V_E$, E macro edge of K, it is not difficult to write down a necessary and

sufficient condition for $\Pi_K^{\nabla,k} v = 0$. Indeed, for $v \in V_E$ we have

$$\int_K \nabla v \cdot \nabla p = \int_E v \nabla p \cdot \nu_K$$

whence

$$v \in \ker \Pi_K^{\nabla,k} \iff \int_E v \nabla p \cdot \nu_K = 0 \quad \text{for all } p \in \mathbb{P}_k.$$

As $\nabla \mathbb{P}_k \subseteq (\mathbb{P}_{k-1})^2$, we also have that

$$\int_E v\vec{p} \cdot \nu_K = 0 \quad \text{for all } \vec{p} = (p_1, p_2) \in (\mathbb{P}_{k-1})^2 \Longrightarrow v \in \ker \Pi_K^{\nabla,k}. \tag{13}$$

We can immediately see that the condition (13) is completely local to the macro edge. Moreover we observe that if E is a macro edge common to K and K', then, as, on E, $\nu_{K'} = -\nu_K$, we have that

$$v \in \ker \Pi_{K'}^{\nabla,k} \Longleftarrow \int_E v\vec{p} \cdot \nu_{K'} = -\int_E v\vec{p} \cdot \nu_K = 0 \quad \text{for all } \vec{p} \in (\mathbb{P}_{k-1})^2,$$

that is the sufficient conditions for having $v|_K \in \ker \Pi_K^{\nabla,k}$ and $v|_{K'} \in \ker \Pi_{K'}^{\nabla,k}$ coincide. We can then split V_E as

$$V_E = \widehat{V}_E \oplus \breve{V}_E \quad \text{with} \quad \breve{V}_E = \{v \in V_E : \int_E v\vec{p} \cdot \nu_E = 0, \ \forall \vec{p} \in (\mathbb{P}_{k-1})^2\},$$

where on a macroedge $E = \partial K \cap \partial K'$ we choose a normal direction, setting either $\nu_E = \nu_K$ or $\nu_E = \nu_{K'}$, and where $\widehat{V}_E$ satisfies $\dim(\widehat{V}_E) + \dim(\breve{V}_E) = \dim(V_E)$. In turn, this results in a splitting of V_H as

$$V_H = \widehat{V}_H \oplus \breve{V}_H, \qquad \text{with } \breve{V}_H = \oplus_E \breve{V}_E, \qquad \widehat{V}_H = V_H^I \oplus V_H^X \oplus_E \widehat{V}_E,$$

where V^I and V^X are, respectively, the space of functions in V_H identically vanishing on all edges of the tessellation $\mathcal{T}_H$ (that is the subspace of functions with vanishing vertex and edges degrees of freedom), and the space spanned by the basis functions corresponding to macro vertex (that is of vertexes of macro edges) degrees of freedom. We observe that for $\breve{v} \in \breve{V}_H$ not only we have that $\Pi^\nabla(\breve{v}) = 0$ (this is by construction), but we also have that $\Pi^0(\breve{v}) = 0$. In a way the functions in $\breve{V}_H$ do not (at least not directly) contribute to the consistency/accuracy of the method, and we then dub them (and the corresponding set of degrees of freedom) as "lazy".

If we test equation (11) with $v = \breve{v} \in \breve{V}_H$ we obtain the following identity

$$S(\widehat{u}_h - \Pi^\nabla(\widehat{u}_h), \breve{v}) + S(\breve{u}_h, \breve{v}) = 0, \quad \text{where} \quad S(\varphi, \psi) = \sum_K S_a^K(\varphi, \psi), \tag{14}$$

from which we immediately obtain

$$\breve{u}_h = -\Pi_S(\widehat{u}_h - \Pi^\nabla(\widehat{u}_h)),$$

where Π_S is the projection onto $\breve{V}_H$, orthogonal with respect to the scalar product $S(\cdot,\cdot)$. We can then plug back this expression in equation (11) and set $v = \widehat{v} \in \widehat{V}_H$, obtaining the following reduced problem in $\widehat{V}_H$

$$\begin{aligned}
&\int_{\mathcal{T}_H} \nabla\Pi^\nabla(\widehat{u}_h) \cdot \nabla\Pi^\nabla(\widehat{v}) - \int_{\partial\Omega_h} \partial_\nu \Pi^\nabla(\widehat{u}_h)\widehat{v} \\
&\quad - \int_{\partial\Omega_h} \left(\Pi^\nabla(\widehat{u}_h) + \mathscr{C}\left[\Pi^\nabla(\widehat{u}_h)\right]\right) \left(\partial_{\nu_h}\Pi^\nabla(\widehat{v}) - \gamma H^{-1}(\Pi^\nabla(\widehat{v}) + \widehat{\mathscr{C}}\left[\Pi^\nabla(\widehat{v})\right])\right) \\
&\qquad + s((1-\Pi_S)(\widehat{u}_h - \Pi^\nabla(\widehat{u}_h)), (1-\Pi_S)(\widehat{v} - \Pi^\nabla(\widehat{v}))) \\
&\quad = \int_{\Omega_h} f\Pi^0(\widehat{v}) - \sum_{e\in\mathcal{E}^\partial} \int_e g^\star \left(\partial_{\nu_h}\Pi^\nabla(\widehat{v}) - \gamma H^{-1}(\Pi^\nabla(\widehat{v}) + \widehat{\mathscr{C}}\left[\Pi^\nabla(\widehat{v})\right])\right),
\end{aligned} \tag{15}$$

where, to make the term involving the stabilization symmetric, we exploited the fact that $1 - \Pi_S$ is the self adjoint projector with respect to the scalar product $S(\cdot,\cdot)$. Remark that, compared to the full formulation in V_H, the only term that is modified is the stabilization term. Moreover, if we choose S in such a way that the corresponding matrix is diagonal, the computation of Π_S turns out to be particularly cheap.

Remark 4.1. As already mentioned before, the method proposed in [2] is slightly different. More precisely, the discrete equation considered in such a paper is the following

$$\begin{aligned}
&a_H(u_h, v) - \int_{\partial\Omega_h} \partial_\nu \Pi^\nabla(\widehat{u}_h)v \\
&\qquad - \int_{\partial\Omega_h} \left(u_h + \mathscr{C}\left[\Pi^\nabla(u_h)\right]\right) \left(\partial_{\nu_h}\Pi^\nabla(v) - \gamma H^{-1}v\right) \\
&\qquad\qquad = \int_{\Omega_h} f\Pi^0(v) - \int_{\partial\Omega_h} g^\star \left(\partial_{\nu_h}\Pi^\nabla(v) - \gamma H^{-1}v\right).
\end{aligned}$$

	Method	$\widehat{k}$	$\sigma(\mathbf{x})$	Ref.
(A)	High order shifted boundary method	1	$\nabla \mathrm{d}(\mathbf{x}, \partial\Omega)$	[1]
(B)	BDT + closest point mapping	0	$\nabla \mathrm{d}(\mathbf{x}, \partial\Omega)$	[20]
(C)	BDT + p.w. constant closest point mapping	0	$\nabla \mathrm{d}(\mathbf{x}_e, \partial\Omega)$	[2]

Table 1: The three boundary correction strategies considered for the numerical tests. For all three methods the extrapolation direction is given by the gradient of the distance to the boundary, which for the (C) case is evaluated at the midpoint of each edge.

With respect to the above formulation, besides considering a more general design of the Nitsche stabilization term, the equation (11) replaces u_h and v on $\partial\Omega_h$ with $\Pi^\nabla(u_h)$ and $\Pi^\nabla(v)$. Without this modification, the static condensation of the "lazy" degrees of freedom would require solving an equation of the form

$$S(\breve{u}_h, \breve{v}) + \gamma H^{-1} \int_{\partial\Omega_h} \breve{u}_h \breve{v} = \int_{\partial\Omega_h} \partial_\nu \Pi^\nabla(\widehat{u}_h) \breve{v} - \gamma H^{-1} \int_{\partial\Omega_h} \left(\widehat{u}_h - \mathscr{C}\left[\Pi^\nabla(\widehat{u}_h)\right]\right) \breve{v} + \gamma H^{-1} \int_{\partial\Omega_h} g^\star \breve{v}$$

instead of the simpler and much cheaper equation (14).

5. Numerical results

We devote this section to test the performance of the virtual element method with boundary correction for increasing values of k, and to compare its performance with the performance of analogous methods in the finite element framework. We consider different variants of the proposed method, as illustrated in Table 1.

We tested the proposed method on two different curved domains, with different characteristics, namely a disk and a bean shaped domain with curved boundary, and a reentrant corner with interior angle equals to $3\pi/2$. We consider different meshes, obtained by agglomerations of squared elements from uniform structured meshes of meshsize h, for different values of the ratio $\widehat{\tau} = h/H$, which, unless otherwise stated, is the same for all the elements of a given mesh. We underline that, as stated in Remark 3.3, the considered tessellations automatically satisfy Assumption 3.2 with $\alpha_1 \lesssim \widehat{\tau}^{-1}$.

Letting u_h denote the discrete solution obtained by the order k VEM method proposed in the previous section, for all the tests we consider the relative error in

the $H^1(\mathcal{T}_H)$ seminorm, as well as in the $L^2(\Omega_h)$ norm. For the VEM case, these are, as usual, approximated as

$$e_1^u := \frac{\|\nabla u - \Pi^0_{k-1}(\nabla u_h)\|_{0,\Omega_h}}{|u|_{1,\Omega_h}}, \qquad e_0^u := \frac{\|u - \Pi^0_k u_h\|_{0,\Omega_h}}{\|u\|_{0,\Omega_h}}, \tag{16}$$

where $\Pi^0_\ell : L^2(\Omega_h) \to \mathbb{P}_\ell(\mathcal{T}_H)$ is the L^2 orthogonal projection onto the space of discontinuous piecewise polynomials of order up to ℓ. For both test cases, we consider values of k between 1 and 6. To facilitate the interpretaton of the results, which, for all tests, we plot in log-log scale, for each set of data we also plot a dotted line which we fit, by linear regression, to the central part of the data set (we exclude one or two values, that we estimate less relevant, at each end). The slope of such a line is reported in the plots.

5.1. Test 1 – Disk domain

For the first test, the domain is the disk of center $(0.5, 0.5)$ and radius 0.5. We solve Problem (1) with data chosen in such a way that the solution u of the problem is the Franke function [63]

$$\begin{aligned} u_{\text{Frnk}}(x,y) := \frac{3}{4}e^{-\left((9x-2)^2+(9y-2)^2\right)/4} + \frac{3}{4}e^{-\left((9x+1)^2/49+(9y+1)/10\right)} \\ + \frac{1}{2}e^{-\left((9x-7)^2+(9y-3)^2\right)/4} + \frac{1}{5}e^{-\left((9x-4)^2+(9y-7)^2\right)}. \end{aligned} \tag{17}$$

As for the boundary correction strategy, we test both the shifted boundary method (strategy (A)) and the Bramble, Dupont and Thomée method with piecewise constant closest point extrapolation direction, as proposed in [2] (strategy (C)). For the sake of comparison, we also present the results of the shifted boundary method and of the Bramble, Dupont, Thomée method with closest point extrapolation direction (strategy (B), proposed in [20]), in combination with order k rectangular finite elements on the structured uniform grid corresponding to the $\widehat{\tau} = 1$ case. For the first set of tests we set the stabilization parameter for the Nitsche's method $\gamma = 100$.

5.1.1. Effect of the refinement paameter $\widehat{\tau}$

We start by testing the order k finite element and virtual element methods with different boundary correction strategies on a sequence of progressively finer quadrangular meshes. For the VEM, which, we recall, yields a different method with respect to finite elements (FE) even on triangular and quadrangular meshes, this corresponds, in our framework, to setting $\widehat{\tau} = 1$. Figure 6 displays the results. The loss of stability as k increases is apparent. This is less pronounced for the VEM

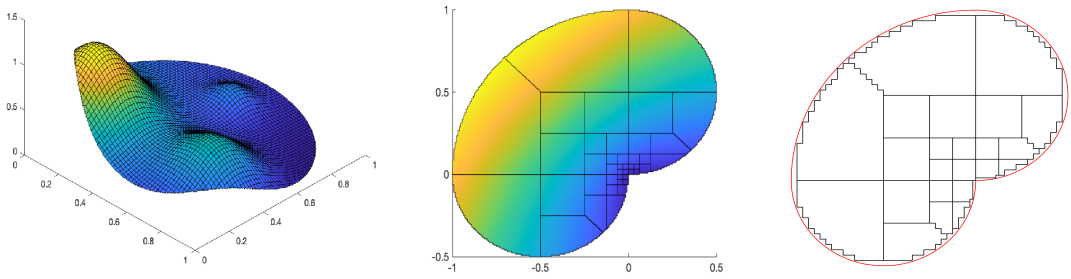


Figure 5: The solution to test problem 2 (top) and one of the meshes used in the tests. Remark that the approximate domain Ω_h is included in Ω.

method than for the two methods based on quadrangular finite elements, due, we believe, to the fact that order k Q-type finite elements are polynomials of order $k+1$, and have, therefore larger inverse inequality constants than the ones for the space $\mathbb{P}_k = \Pi_K^{\nabla,k}(V^{K,k})$. Nevertheless, also for the two virtual element methods, we see some instabilities for $k = 5$ and $k = 6$. We also observe that for the VEM method, owing, we believe, to the shifted boundary method choice of the stabilization, strategy (A) appears to be more stable than strategy (C).

Switching to polygonal elements, and focusing on VEM, the situation improves as we take smaller values of $\widehat{\tau}$. In Figures 7 and 8 we present the results of our test on polygonal meshes obtained by agglomeration of uniform square meshes, for $\widehat{\tau} = 0.5$, 0.25 and 0.125. As $\widehat{\tau}$ decreases, the instabilities progressively disappear and, for $\widehat{\tau} = .125$, the behavior of the H^1 error for both strategies (A) and (C) appears optimal for all ks in our range (we believe the increase of the error for $k = 6$ on the finest mesh to be the result of round-off errors). We can however still see some slight oscillations in the L^2 norm for strategy (C). We also tested lower values of $\widehat{\tau}$, namely 0.0625 and 0.03125, with similar results.

5.1.2. Effect of the choice of the stabilization parameter γ

It is well known that the performance of Nitsche's method is affected by the choice of the stabilization parameter γ. The theoretical analysis of our method confirms that, also in our case, this has to be chosen large enough, that is, larger than γ_0 that depends on k (tracking the dependence on k in the analysis of the method suggests that $\gamma_0 \simeq \bar{\gamma}k^2$ for some positive $\bar{\gamma}$). To assess how sensitive to the choice of γ the method actually is, we tested, for the case $\widehat{\tau} = 0.125$, three values of γ, namely, $\gamma = 10$, $\gamma = 100$ and $\gamma = 150$. Figures 9 and 10 suggest that $\gamma = 10$ is too low for $k > 2$, while $\gamma = 100$ is good up to $k = 5$, but too low for $k = 6$, for which

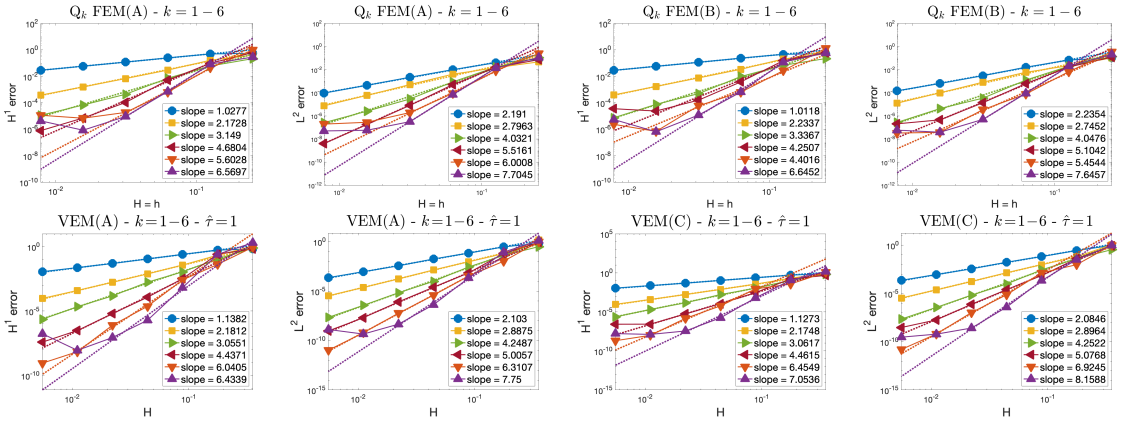


Figure 6: Test case 1, test on quadrangular meshes: H^1 and L^2 error for Q_k finite element with boundary correction strategies (A) and (B) (top), in comparison with VEM with boundary correction strategies (A) and (C) on the same rectangular meshes (bottom). The stabilization parameter for Nitsche's method is $\gamma = 100$.

$\gamma = 150$ yields instead, optimal results for both strategies (A) and (C). We also observe that increasing γ does not seem to negatively affect the error, and then it seems reasonable, in the absence of a more precise analysis on the dependence of such a constant on the different parameters of the method, such as the one presented in [1], to err on the side of caution and choose γ larger rather than smaller.

5.1.3. Robustness with respect to the parameter $\widehat{\tau}$

We aim at demonstrating that, by applying the static condensation procedure proposed in Section 4, it is possible to lower the value of the parameter τ without asymptotically increasing the number of degrees of freedom. In Figure 11 we plot, for $k = 1, \cdots, 6$ the number of active degrees of freedoms retained after the elimination of the lazy degrees of freedom by the approach presented in Section 4, for the meshes used for all the tests of Sections 5.1 and 5.2. Observe how, for H sufficiently small and $\tau \leqslant .25$ the curves are, for all values of k essentially superposed, that is, the number of degrees of freedom for a given value of H does not increase as τ goes to 0. For all k it is therefore possible to choose such a parameter in such a way that the resulting method is stable, without increasing the size of the linear system to be solved.

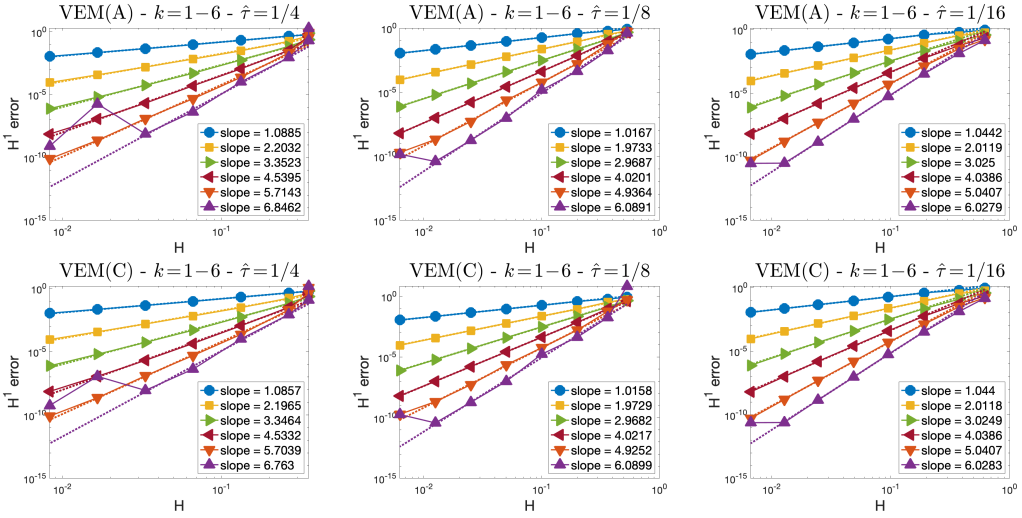


Figure 7: Test case 1, H^1 convergence of the VEM method with boundary correction strategies (A) and (C) for $k = 1, \cdots, 6$, with different values of $\widehat{\tau} = h/H$. For $\widehat{\tau} = 1$ and $k \geqslant 5$ the method displays evident instabilities. For $\widehat{\tau} = .5$ the method is only slightly suboptimal. For $\widehat{\tau} \leqslant .25$ we observe an optimal behavior for all $k \leqslant 5$, and only some very mild oscillations for $k = 6$. The dotted lines are obtained by linear regression fitting to a subset of the data that excludes the coarsest as well as the two finest meshes.

5.2. Test 2 – Bean domain

In this test we consider a domain with a corner with interior angle equals to $3\pi/2$, obtained as the union of a quarter of a disk with two half disks:

$$\Omega = \Omega_1 \cup \Omega_2 \cup \Omega_3 \quad \text{with} \quad \begin{cases} \Omega_1 = \{(x,y) : (x^2+y^2) < 1,\ x < 0, y > 0\}, \\ \Omega_2 = \{(x,y) : (x+.5)^2 + y^2 < 0.25, x < 0\}, \\ \Omega_3 = \{(x,y) : x + (y-.5)^2 < 0.25, x < 0\}. \end{cases}$$

The load and the non homogeneous Dirichlet data are chosen so that the solution (see Figure 5), expressed in polar coordinates, is

$$u(\rho, \vartheta) = \rho^{2/3} \sin(2\vartheta/3),$$

a standard benchmark for corner singularities. We know that $u \in H^s(\Omega)$ for all $s < 3/2$, but $u \notin H^{3/2}(\Omega)$. As we are in the presence of an interior angle, we follow an *hp* strategy by resorting to geometric meshes, progressively refined in the proximity of the singular point $(0,0)$, while simultaneously increasing the order of the method. In the case of a polygonal domain, this strategy is expected to yield an

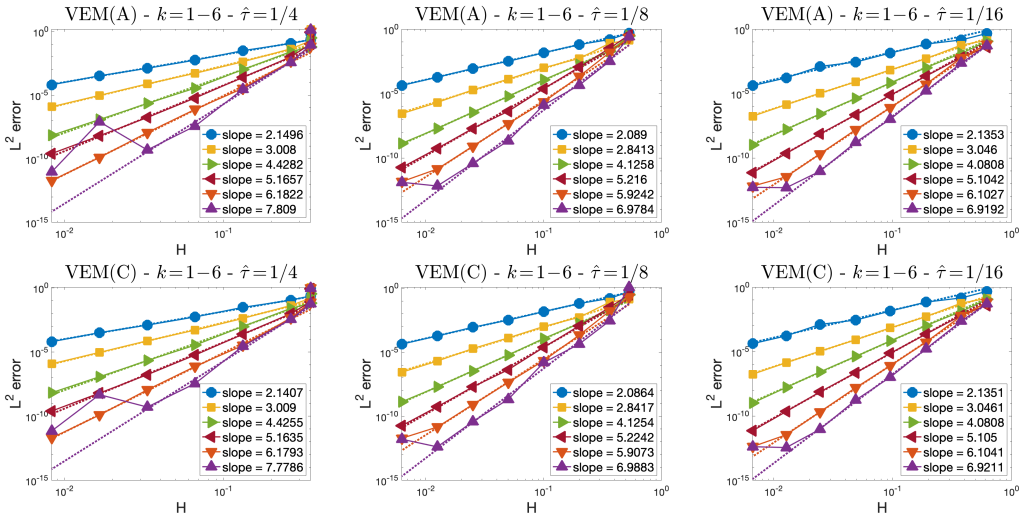


Figure 8: Test case 1, L^2 convergence of the VEM method with boundary correction strategies (A) and (C) for $k = 1, \cdots, 6$, with different values of $\widehat{\tau} = h/H$. The dotted lines are obtained by linear regression fitting to a subset of the data that excludes the coarsest as well as the two finest meshes. The behavior is similar to the one of the H^1 norm.

exponential convergence of the $H^1(\Omega_h)$ error satisfying the bound

$$\|u - u_h\|_{1,\Omega_h} \lesssim \exp(-\sqrt[3]{N}),$$

where N is the number of degrees of freedom [64]. Observing that the parameter τ_γ and γ_0 given by Theorem 3.6 depend on k and that a rough analysis suggests that $\tau_\gamma \simeq 1/k^2$ and $\gamma_0 \simeq k^2$, as the order of the method increases, we decrease h so that the first condition is satisfied, and possibly modify also the elements that are not refined, enlarging them through the union of squared elements of the finer squared mesh with meshsize h. We refer to this adjustment of the elements close to the boundary as δ refinement. Simultaneously, we adjust the stabilization parameter and set $\gamma = \bar{\gamma}k^2$.

Once again, we consider the virtual element method with both strategy (A) and (C) boundary correction, and we test different values of the parameter $\bar{\gamma}$. The results, presented in Figure 12, display a behaviour similar to the one obtained for polygonal domains, where no boundary correction is needed. This suggests that, in the framework of the virtual element method, that allows to adjust the distance of the approximate and true boundary by reducing the mesh size of the fine grid $\mathcal{T}_h$, boundary correction approaches such as the shifted boundary method or the BDT method with closest point mapping are potentially applicable in the $h-p$ framework.

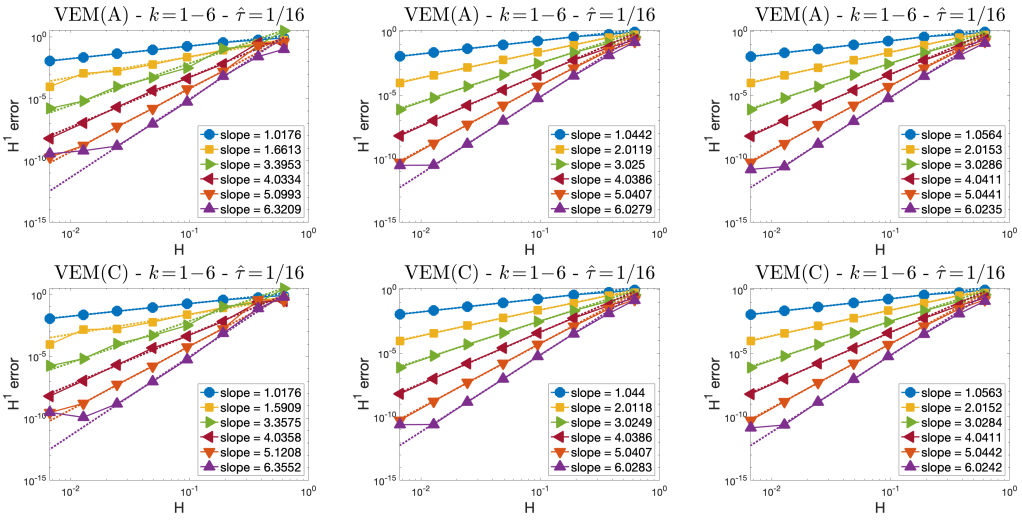


Figure 9: Test case 1 - Effect of the choice of the Nitsche stabilization parameter γ. H^1 error for the VEM method with boundary correction strategies (A) (top) and (C) (bottom). From left to right, $\gamma = 10$ (first column), $\gamma = 100$ (central column), $\gamma = 150$ (last column). For all tests we have $\hat{\tau} = 1/16$.

6. Conclusions and perspectives

We evaluated the performance of a boundary corrected virtual element method, for the numerical solution of the Poisson equation on curved smooth domain approximated by a polygonal domain of the type that can be easily built out of images (i.e. domain obtained as the union of pixels). The use of polygonal elements obtained as agglomeration of pixels allows boundary correction methods such as the shifted boundary method to satisfy the assumptions guaranteeing stability and optimality of the error estimates for arbitrary values of the order of the method. Eliminating, by a cheap static condensation procedure, a large number of degrees of freedom that do not actively contribute to the consistency of the method, allows to retrieve a robust behaviour of the error as a function of the number of degrees of freedom, independently of the order of approximation, that can be arbitrarily high. The numerical results demonstrate the potential of the method. While the paper only deals with the two dimensional case, the method is well suited to be applied also in three dimension ([54]), though in such a case, in the elimination of the "lazy" degrees of freedom extra care will be needed to deal with the wirebasket. The method is well suited to be eventually coupled with an adaptive reconstruction of the smooth continuous boundary from imaging data, which, together with the extension to three dimensions, will be the focus of a forthcoming paper.

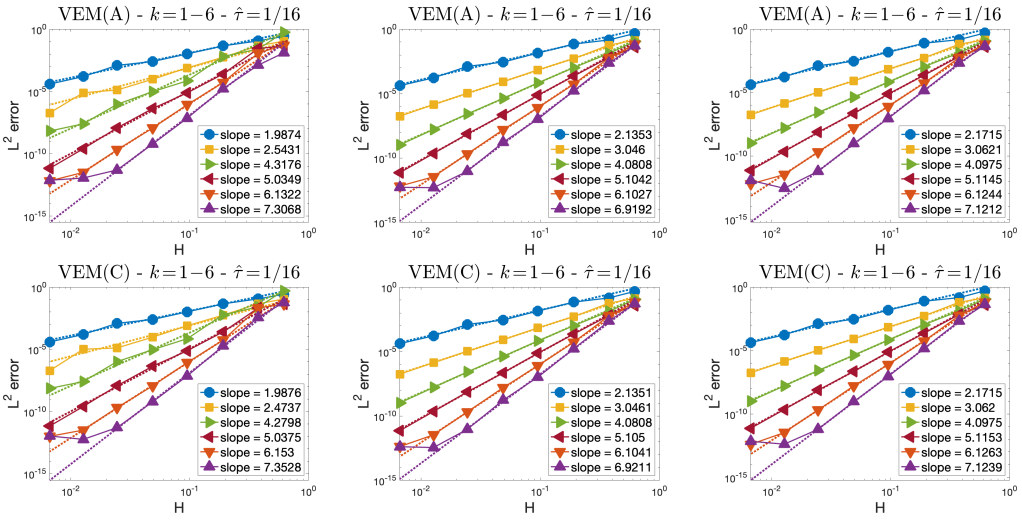


Figure 10: Test case 1 - Effect of the choice of the Nitsche stabilization parameter γ. L^2 error for the VEM method with boundary correction strategies (A) (top) and (C) (bottom). From left to right, $\gamma = 10$ (first column), $\gamma = 100$ (central column), $\gamma = 150$ (last column). For all tests we have $\hat{\tau} = 1/16$.

Appendix A. Proof of Lemma 3.4

We let (a, b), $a < b$, denote the interval of extrema a and b. We start by observing that, under our assumptions, the elements K in our mesh are extension domains ([65]). We can then embed them in a square of diameter $\simeq H$, which, for simplicity, we will assume to be the square $\widehat{S} = (0, H)^2$, and, for all $v \in H^1(K)$ there exists $\widehat{v} \in H^1(\widehat{S})$ with $\|\widehat{v}\|_{1,\widehat{S}} \lesssim \|v\|_{1,K}$, the constant in the inequality independent of H and h. Moreover, a Poincaré inequality holds in K, of the form

$$\inf_{\alpha \in \mathbb{R}} \|v - \alpha\|_{0,K} \lesssim H|v|_{1,K}$$

with constants independent of H and h. For $v \in C^1(\bar{K})$ we can write

$$\|v\|^2_{0,\partial\Omega_h} = \sum_{e \in \mathcal{E}^K_{\text{hor}}} \|v\|^2_{0,e} + \sum_{e \in \mathcal{E}^K_{\text{ver}}} \|v\|^2_{0,e},$$

where $\mathcal{E}^K_{\text{hor}} \subset \mathcal{E}^K$ and $\mathcal{E}^K_{\text{ver}} \subset \mathcal{E}^K$ are the sets of, respectively, horizontal and vertical edges of K. Let us consider the contribution of vertical edges. We have, with $e = \{x_e\} \otimes (y^0_e, y^1_e)$,

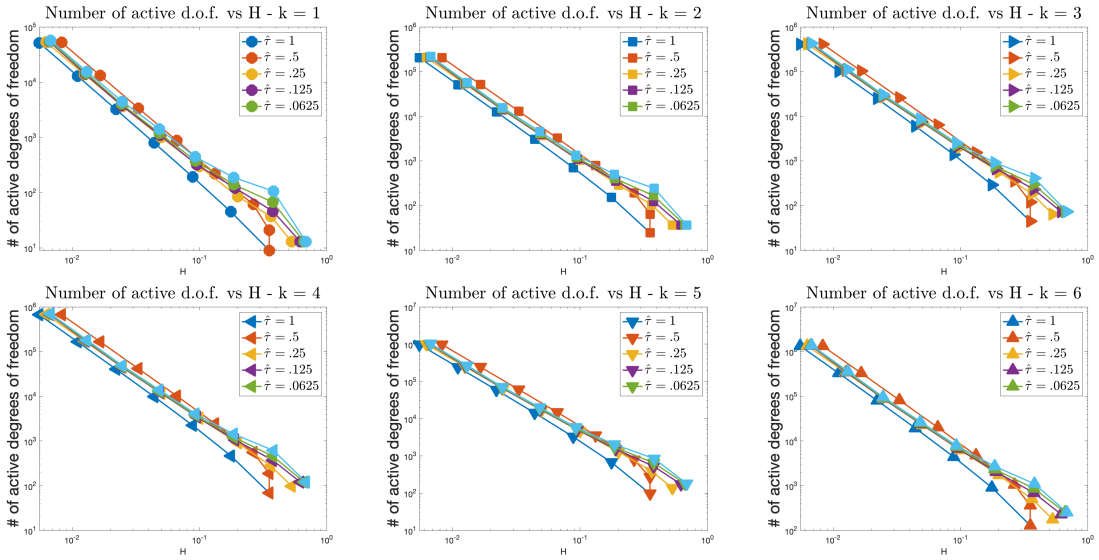


Figure 11: Number of active degrees of freedom (independent of the chosen boundary correction strategy) for the meshes used for the tests on the disk domain, for different values of the order k of the method and of the refinement parameter τ.

$$\sum_{e\in\mathcal{E}^K_{\text{ver}}} \|v\|^2_{0,e} = \sum_{e\in\mathcal{E}^K_{\text{ver}}} \int_{y_e^0}^{y_e^1} |v(x_e,y)|^2\,dy \lesssim \sum_{e\in\mathcal{E}^K_{\text{ver}}} \int_{y_e^0}^{y_e^1} ||K|^{-1}\int_K v(\sigma,\tau)\,d\sigma\,d\tau|^2\,dy$$
$$+ \sum_{e\in\mathcal{E}^K_{\text{ver}}} \int_{y_e^0}^{y_e^1} |v(x_e,y) - |K|^{-1}\int_K v(\sigma,\tau)\,d\sigma\,d\tau|^2\,dy = I + II.$$

We can write

$$I \lesssim \sum_{e\in\mathcal{E}^K_{\text{ver}}} \int_{y_e^0}^{y_e^1} |K|^{-1}\int_K |v(\sigma,\tau)|^2\,d\sigma\,d\tau\,dy \leqslant \frac{|\partial K|}{|K|}\|v\|^2_{0,K} \lesssim H^{-1}\|v\|^2_{0,K}.$$

Now we have

$$II = \sum_{e\in\mathcal{E}^K_{\text{ver}}} \int_{y_e^0}^{y_e^1} ||K|^{-1}\int_K (v(x_e,y) - v(\sigma,\tau))\,d\sigma\,d\tau|^2\,dy$$
$$\leqslant \sum_{e\in\mathcal{E}^K_{\text{ver}}} \int_{y_e^0}^{y_e^1} ||K|^{-1}\int_K (v(x_e,y) - \widehat{v}(\sigma,y))\,d\sigma\,d\tau|^2\,dy$$
$$+ \sum_{e\in\mathcal{E}^K_{\text{ver}}} \int_{y_e^0}^{y_e^1} ||K|^{-1}\int_K (\widehat{v}(\sigma,y) - v(\sigma,\tau))\,d\sigma\,d\tau|^2\,dy = III + IV.$$

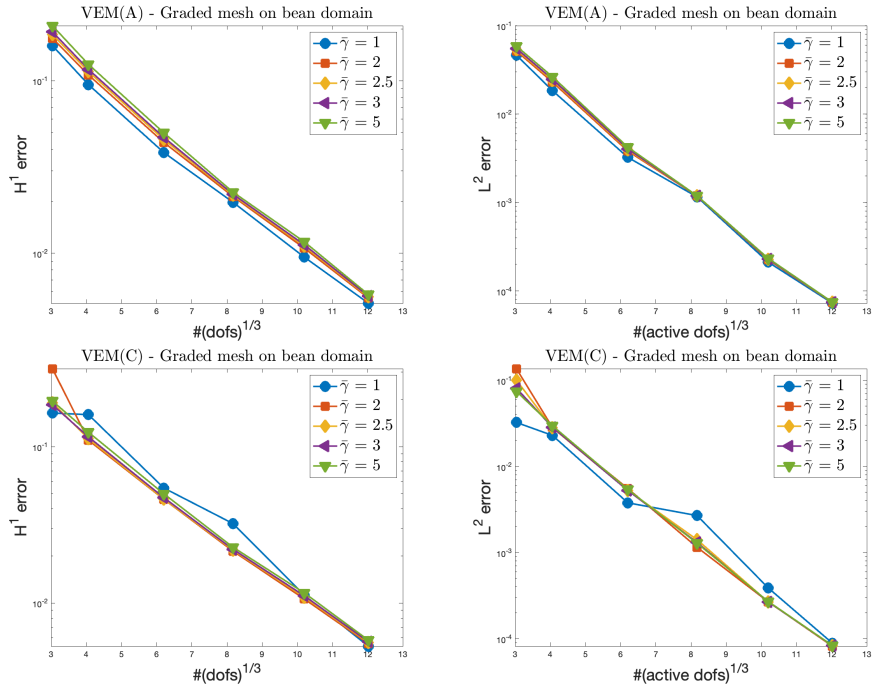


Figure 12: Test case 2. Convegence of the VEM method with boundary correction strategies (A) and (C), for a singular solution, with a graded mesh and both $h-p$ and δ refinement.

.

We can bound III as

$$
\begin{aligned}
III &\lesssim \sum_{e\in\mathcal{E}^K_{\mathrm{ver}}} \int_{y_e^0}^{y_e^1} |K|^{-1} \int_K |(v(x_e,y)-\widehat{v}(\sigma,y))|^2 \, d\sigma \, d\tau \, dy \\
&= \sum_{e\in\mathcal{E}^K_{\mathrm{ver}}} \int_{y_e^0}^{y_e^1} |K|^{-1} \int_K |\int_\sigma^{x_e} \partial_x \widehat{v}(\xi,y)\, d\xi|^2 \, d\sigma \, d\tau \, dy \\
&\lesssim \sum_{e\in\mathcal{E}^K_{\mathrm{ver}}} \int_{y_e^0}^{y_e^1} |K|^{-1} \int_K |x_e-\sigma| \int_\sigma^{x_e} |\partial_x \widehat{v}(\xi,y)|^2 \, d\xi \, d\sigma \, d\tau \, dy \\
&\leqslant |K|^{-1} \int_K H \sum_{e\in\mathcal{E}^K_{\mathrm{ver}}} \int_{y_e^0}^{y_e^1} \int_0^H |\partial_x \widehat{v}(\xi,y)|^2 \, d\xi \, dy \, d\sigma \, d\tau \\
&\lesssim H \sum_{e\in\mathcal{E}^K_{\mathrm{ver}}} \int_{y_e^0}^{y_e^1} \int_0^H |\partial_x \widehat{v}(\xi,y)|^2 \, d\xi \, dy \leqslant H \|\partial_x \widehat{v}\|^2_{0,\widehat{S}},
\end{aligned}
$$

while IV is bound as

$$
\begin{aligned}
IV &\lesssim \sum_{e\in\mathcal{E}^K_{\mathrm{ver}}} \int_{y_e^0}^{y_e^1} |K|^{-1} \int_K |(v(\sigma,y)-\widehat{v}(\sigma,\tau))|^2 \, d\sigma \, d\tau \, dy \\
&= \sum_{e\in\mathcal{E}^K_{\mathrm{ver}}} \int_{y_e^0}^{y_e^1} |K|^{-1} \int_K |\int_\tau^{y} \partial_y \widehat{v}(\sigma,\zeta)\, d\zeta|^2 \, d\sigma \, d\tau \, dy \\
&\lesssim \sum_{e\in\mathcal{E}^K_{\mathrm{ver}}} \int_{y_e^0}^{y_e^1} |K|^{-1} \int_{\widehat{S}} |y-\tau| \int_\tau^{y} |\partial_y \widehat{v}(\sigma,\zeta)|^2 \, d\zeta \, d\sigma \, d\tau \, dy \\
&\lesssim \sum_{e\in\mathcal{E}^K_{\mathrm{ver}}} \int_{y_e^0}^{y_e^1} H|K|^{-1} \int_0^H \int_0^H \int_0^H |\partial_y \widehat{v}(\sigma,\zeta)|^2 \, d\zeta \, d\sigma \, d\tau \, dy \lesssim H \|\partial_y \widehat{v}\|^2_{0,\widehat{S}},
\end{aligned}
$$

finally yielding

$$
II \lesssim III + IV \lesssim H|\widehat{v}|^2_{1,\widehat{S}} \lesssim H|v|^2_{1,K}.
$$

The contribution of horizontal edges is bound by the same argument, allowing to conclude that (5) holds for v smooth. The result for a generic $v \in H^1(K)$ is obtained by density. The bound (6) for polynomials is a direct consequence of the combination of the previous bound with the inverse inequality

$$
\|p\|_{1,S(\mathbf{x}_K,H_K)} \lesssim H^{-1} \|p\|_{0,S(\mathbf{x}_K,\alpha_1 H)}.
$$

In order to prove (7), we rely on the triangulation $\widetilde{\mathcal{T}}_K$ provided by Assumption 3.2. For each edge $e \in \mathcal{E}^K$ we let $T_e \in \widetilde{\mathcal{T}}_K$ denote the triangle having e as an edge. Thanks to the shape regularity of the triangulation we can write $|v|_{r-1/2,e} \lesssim |v|_{r,T_e}$, the implicit constant in the inequality only depending on the constant α_1. Then

$$\sum_{e\in\mathcal{E}^K} |v|^2_{r-1/2,e} \lesssim \sum_{e\in\mathcal{E}^K} |v|^2_{r,T_e} \lesssim \sum_{T\in\widetilde{\mathcal{T}}_K} |v|^2_{r,T} \lesssim |v|^2_{r,K}.$$

Appendix B. Proof of Lemma 3.5

Given $u \in H^s(K)$, $2 \leqslant s \leqslant k+1$, we aim at constructing a quasi interpolant $u_I \in V^{K,k}$ such that we can prove an optimal estimate on $u - u_I$, robust in h and H. We start by recalling that for all $v \in H^{1/2}(\partial K)$ it holds that

$$\inf_{\substack{\varphi\in H^1(K)\\ \varphi = v \text{ on } \partial K}} |\varphi|_{1,K} = |\mathcal{H}(v)|_{1,K},$$

where $\mathcal{H}(u)$ denotes the harmonic lifting of u. We can then consider, for $H^{1/2}(\partial K)$ the non standard norm

$$|\!|\!| v |\!|\!|_{1/2,\partial K} = |\mathcal{H}(v)|_{1,K} + \|v\|_{0,\partial K}.$$

We now let W^K denotes the standard finite element space of continuous piecewise polynomial functions of degree at most k defined on the auxiliary triangulation $\widetilde{\mathcal{T}}_K$ given by Assumption 3.2. Then, given $v \in \mathbb{B}_k(\partial K)$ and letting $\widetilde{v} \in W^K$ denote the order k finite element function coinciding with v on ∂K and vanishing at all nodes interior to K, we can write that

$$|\mathcal{H}(v)|^2_{1,K} \leqslant |\widetilde{v}|^2_{1,K} = \sum_{K\in\widetilde{\mathcal{T}}_K} |\widetilde{v}|^2_{1,T} = \sum_{e\in\mathcal{E}^K} |\widetilde{v}|^2_{1,T_e} \lesssim \sum_{e\in\mathcal{E}^K} h_e^{-1} \|\widetilde{v}\|^2_{0,e}, \tag{B.1}$$

where we exploited the fact that $\widetilde{v}$ vanishes on all interior triangles, and where the last inequality is obtained by a standard inverse inequality for order k polynomials on T_e. Letting $|\!|\!| \cdot |\!|\!|_{-1/2,\partial K}$ be defined as

$$|\!|\!| \varphi |\!|\!|_{-1/2,\partial K} = \sup_{\substack{v\in H^{1/2}(\partial K)\\ \int_{\partial K} v = 0}} \frac{\int \varphi v}{|\!|\!| v |\!|\!|_{1/2,\partial K}},$$

we easily see that, for $v \in H^1(K)$ with $\Delta v \in L^2(K)$, Δv average free, it holds, uniformly in h and H, that

$$\|\!|\nabla v \cdot \nu_K|\!\|_{-1/2,\partial K} \lesssim \|\Delta v\|_{(H^1(K)/\mathbb{R})'} + |v|_{1,K}. \tag{B.2}$$

For $u \in H^s(K)$, $2 \leqslant s \leqslant k+1$ we now let $\widetilde{u}_I \in \widetilde{V}^{K,k}$ be defined as

$$\widetilde{u}_I(x_i) = u(x_i) \text{ for all node } x_i \text{ of } \mathcal{T}_H, \quad \text{and} \quad \int_K \Delta(u - \widetilde{u}_I) q = 0 \text{ for all } q \in \mathbb{P}_k(K),$$

and we define $u_I \in V^{K,k}$ as

$$u_I = \widetilde{u}_I \text{ on } \partial K \qquad \text{and} \qquad \int_K (u_I - \widetilde{u}_I) q = 0 \text{ for all } q \in \mathbb{P}_{k-2}(K).$$

We claim that u_I thus defined satisfies (9). Let us start by bounding $|u - \widetilde{u}_I|_{1,K}$. Integrating by parts, using (B.2) and the inverse inequality (B.1), as well as an Aubin Nitsche type duality trick to bound the $(H^1(K)/\mathbb{R})'$ norm of $\Delta(u - \widetilde{u}_I)$, plus some standard polynomial interpolation bound on each edge, we can write

$$\begin{aligned}
|u - \widetilde{u}_I|_{1,K}^2 &= -\int_K (\Delta(u - \widetilde{u}_I))(u - \widetilde{u}_I) + \int_{\partial K} \nabla(u - \widetilde{u}_I) \cdot \nu_K (u - \widetilde{u}_I) \\
&\lesssim \|\Delta(u - \widetilde{u}_I)\|_{(H^1(K)/\mathbb{R})'} |u - \widetilde{u}_I|_{1,K} + \|\!|\nabla(u - \widetilde{u}_I) \cdot \nu_K|\!\|_{-1/2,\partial K} \|\!|u - \widetilde{u}_I|\!\|_{1/2,\partial K} \\
&\lesssim \|\Delta(u - \widetilde{u}_I)\|_{(H^1(K)/\mathbb{R})'} \left(|u - \widetilde{u}_I|_{1,K} + \|u - \widetilde{u}_I\|_{0,\partial K} \right) \\
&+ |u - \widetilde{u}_I|_{1,k} \left(\sum_{e \in \mathcal{E}^K} h_e^{-1} \|u - \widetilde{u}_I\|_{0,e}^2 \right)^{1/2} \lesssim H^{s-1} |u|_{s,K} |u - \widetilde{u}_I|_{1,K} + H^{2s-3/2} |v|_{s,K}^2,
\end{aligned}$$

yielding, for $\varepsilon > 0$ arbitrary and for some positive constants C, C' only depending on the shape regularity parameters and on s,

$$|\nabla(u - \widetilde{u}_I)|_{1,K}^2 \leqslant \frac{C}{2\varepsilon} H^{2s-2} |u|_{s,K}^2 + \frac{C\varepsilon}{2} |u - \widetilde{u}_I|_{1,K}^2.$$

Choosing $\varepsilon = 1/C$ yields the bound

$$|u - \widetilde{u}_I|_{1,K} \lesssim H^{s-1} |u|_{s,K}.$$

We now need to bound $|\widetilde{u}_I - u_I|_{1,K}$. Letting $\pi_\ell : L^2(K) \to \mathbb{P}_\ell(K)$ denote the orthogonal projection onto the space of polynomials of degree at most ℓ on K, integrating by parts and using the fact that both $\Delta \widetilde{u}_I$ and Δu_I are polynomials of degree at most k and that $\widetilde{u}_I - u_I$ is orthogonal to $\mathbb{P}_{k-2}(K)$, we have

$$
\begin{aligned}
|\widetilde{u}_I - u_I|_{1,K}^2 &= -\int_K \Delta(\widetilde{u}_I - u_I)(\widetilde{u}_I - u_I) \\
&= \int_K (\pi_k(\Delta(\widetilde{u}_I - u_I)) - \pi_{k-2}(\Delta(\widetilde{u}_I - u_I)))(\widetilde{u}_I - u_I) \\
&= \int_K (\pi_k(\Delta(\widetilde{u}_I - u_I)) - \pi_{k-2}(\Delta(\widetilde{u}_I - u_I)))(\widetilde{u}_I - \Pi_K^{\nabla,k}\widetilde{u}_I)
\end{aligned}
$$

where the last identity descend from the definition of u_I. We now add and subtract $\Delta(\widetilde{u}_I - u_I)$ in the first term of the product within the integral, and u in the second term and we obtain

$$
\begin{aligned}
|\widetilde{u}_I - u_I|_{1,K} \lesssim \|(1-\pi_k)\Delta(\widetilde{u}_I - u_I)\|_{(H^1(K)/\mathbb{R})'}|\widetilde{u}_I - u|_{1,K} \\
+ \lesssim \|(1-\pi_{k-2})\Delta(\widetilde{u}_I - u_I)\|_{(H^1(K)/\mathbb{R})'}|\widetilde{u}_I - u|_{1,K} \\
+ \|(1-\pi_k)\Delta(\widetilde{u}_I - u_I)\|_{(H^1(K)/\mathbb{R})'}|\Pi_K^{\nabla,k}\widetilde{u}_I - u|_{1,K} \\
+ \|(1-\pi_{k-2})\Delta(\widetilde{u}_I - u_I)\|_{(H^1(K)/\mathbb{R})'}|\Pi_K^{\nabla,k}\widetilde{u}_I - u|_{1,K}.
\end{aligned}
$$

Using an Aubin-Nitsche's duality argument, a polynomial approximation bound and an inverse inequality for polynomials, we bound, for $\ell = k, k-2$

$$
\begin{aligned}
\|(1-\pi_\ell)\Delta(\widetilde{u}_I - u_I)\|_{(H^1(K)/\mathbb{R})'} &\lesssim H\|(1-\pi_\ell)\Delta(\widetilde{u}_I - u_I)\|_{0,K} \\
&\lesssim H\|\Delta(\widetilde{u}_I - u_I)\|_{0,K} \lesssim |\widetilde{u}_I - u_I|_{1,K}.
\end{aligned}
$$

Moreover, adding and subtracting u and using a polynomial approximation bound, we have

$$
\begin{aligned}
|\Pi_K^{\nabla,k}\widetilde{u}_I - u|_{1,K} &\leqslant |\Pi_K^{\nabla,k}(\widetilde{u}_I - u) + (u - \Pi_K^{\nabla,k}u)|_{1,K} \\
&\leqslant |\widetilde{u}_I - u|_{1,K} + |u - \Pi_K^{\nabla,k}u|_{1,K} \lesssim H^{s-1}|u|_{s,K}.
\end{aligned}
$$

Combining the different bounds and using a triangular inequality yields the desired bound.

Appendix C. Proof of Theorem 3.6

From Lemma 3.4, we immediately obtain that, for all $\varphi \in V^{K,k}$

$$
\|\partial_{\nu_h}\Pi_K^{\nabla,k}(\varphi)\|_{0,\partial K} \leqslant \|\nabla\Pi_K^{\nabla,k}(\varphi)\|_{0,\partial K} \lesssim H^{-1/2}\|\nabla\Pi_K^{\nabla,k}(\varphi)\|_{0,K},
$$

as well as

$$\|\partial_\sigma^j \Pi_K^{\nabla,k}(\varphi)\|_{0,\partial K} \lesssim H^{1/2-j}\|\nabla \Pi_K^{\nabla,k}(\varphi)\|_{0,K}.$$

Then, it is not difficult to prove that the following bounds hold

$$\|\mathscr{C}\left[\Pi^\nabla(\varphi)\right]\|_{0,\partial\Omega_h} + \|\widehat{\mathscr{C}}\left[\Pi^\nabla(\varphi)\right]\|_{0,\partial\Omega_h} \leqslant C_1 \frac{h}{H}\sqrt{H}|\Pi^\nabla(\varphi)|_{1,\mathcal{T}_H}, \tag{C.1}$$

$$\|\partial_{\nu_h}\Pi_K^{\nabla,k}(\varphi)\|_{0,\partial\Omega_h} \leqslant C_2 H^{-1/2}|\Pi^\nabla(\varphi)|_{1,\mathcal{T}_H}, \tag{C.2}$$

$$\|\varphi - \Pi^\nabla(\varphi)\|_{0,\partial\Omega_h} \leqslant C_3 H^{1/2}|\varphi - \Pi^\nabla(\varphi)|_{1,\mathcal{T}_H} \tag{C.3}$$

(we recall that the boundary correction operators $\mathscr{C}[\cdot]$ and $\widehat{\mathscr{C}}[\cdot]$ are defined in (4)).

Let now $\mathcal{A}_H$ be defined as

$$\begin{aligned}\mathcal{A}_H(\varphi,\psi) = a_H(\varphi,\psi) &- \int_{\partial\Omega_h} \partial_{\nu_h}\Pi^\nabla(\varphi)\psi \\ &- \int_{\partial\Omega_h}\left(\Pi^\nabla(\varphi) + \mathscr{C}\left[\Pi^\nabla(\varphi)\right]\right)\left(\partial_{\nu_h}\Pi^\nabla(\psi) - \gamma H^{-1}\widehat{\mathscr{C}}\left[\Pi^\nabla(\psi)\right]\right).\end{aligned} \tag{C.4}$$

Continuity of the bilinear form $\mathcal{A}_H$ with respect to the norm $|||\cdot|||_{\Omega_h}$ follows from the above bounds. Let us prove that, provided $h/H < \tau$ with τ small enough, the bilinear form $\mathcal{A}_H$ is also coercive. Letting

$$\widehat{\mathscr{E}}[w] = w + \widehat{\mathscr{C}}[w] = \sum_{j=1}^{\hat{k}} \frac{\delta^j}{j!}\partial_\sigma^j w, \quad \text{and} \quad \widehat{\mathscr{D}}[w] = \mathscr{C}[w] - \widehat{\mathscr{C}}[w] = \sum_{j=\hat{k}+1}^{k} \frac{\delta^j}{j!}\partial_\sigma^j w,$$

we can write, for $\varepsilon > 0$ arbitrary

$$\begin{aligned}\mathcal{A}_H(\varphi,\varphi) &\geqslant |\Pi^\nabla(\varphi)|^2_{1,\mathcal{T}_H} + \beta c_*|\varphi - \Pi^\nabla(\varphi)|^2_{1,\mathcal{T}_H} + \gamma H^{-1}\|\widehat{\mathscr{E}}[\Pi^\nabla(\varphi)]\|^2_{0,\partial\Omega_h} \\ &- \int_{\partial\Omega_h}\partial_{\nu_h}\Pi^\nabla(\varphi)(\varphi - \Pi^\nabla(\varphi)) - 2\int_{\partial\Omega_h}\partial_{\nu_h}\Pi^\nabla(\varphi)\widehat{\mathscr{E}}[\Pi^\nabla(\varphi)] - \int_{\partial\Omega_h}\widehat{\mathscr{D}}[\Pi^\nabla(\varphi)]\partial_{\nu_h}\Pi^\nabla(\varphi) \\ &\quad + \int_{\partial\Omega_h}\partial_{\nu_h}\Pi^\nabla(\varphi)\widehat{\mathscr{C}}\left[\Pi^\nabla(\varphi)\right] + \gamma H^{-1}\int_{\partial\Omega_h}\widehat{\mathscr{D}}[\Pi^\nabla(\varphi)]\widehat{\mathscr{E}}[\Pi^\nabla(\varphi)] \\ &\geqslant \big(\frac{1}{2} - C_2^2\varepsilon - \frac{\gamma}{2}C_1^2\tau^2 - (C_1^2 + C_2^2)\tau\big)|\Pi^\nabla(\varphi)|^2_{1,\mathcal{T}_H} + \big(\beta c_* - \frac{C_3^2}{4\varepsilon}\big)|\varphi - \Pi^\nabla(\varphi)|^2_{1,\mathcal{T}_H} \\ &\quad + \big(\frac{\gamma}{2} - 2C_2^2\big)H^{-1}\|\widehat{\mathscr{E}}[\Pi^\nabla(\varphi)]\|^2_{0,\partial\Omega_h}.\end{aligned} \tag{C.5}$$

We now choose $\varepsilon = 1/(4C_2^2)$ and let $\beta_0 = C_3^2/(4c_*\varepsilon)$ and $\gamma_0 = 4C_2^2$, in such a way that for $\beta > \beta_0$ and $\gamma > \gamma_0$ we have $\beta c_* - C_3^2/(4\varepsilon) > 0$ and $\gamma/2 - 2C_2^2 > 0$. For $\gamma > \gamma_0$, let now $\tau_0(\gamma)$ denote the only positive solution of the equation $\frac{1}{2} - \frac{\gamma}{2}C_1^2\tau^2 - (C_1^2 + C_2^2)\tau = 0$. We easily see that for $\tau < \tau_0(\gamma)$, the coefficients of the first terms on the right hand side of (C.5) is strictly positive and the bilinear form $\mathcal{A}_H$ is, therefore, coercive with respect to the norm $|||\cdot|||_{\Omega_h}$. An unique discrete solution u_h does thus exist.

Let u_I denote the VEM interpolant given by Lemma 3.5 and $u_\pi \in \mathbb{P}_k(\mathcal{T}_H)$ the $L^2(\Omega)$ projection of u onto the space of discontinuous piecewise polynomials, and set $d_h = u_I - u_h$. As in [24], we obtain

$$|||u_I - u_h|||_{\Omega_h}^2 \lesssim |E1| + |E2| + |E3| + |E4| + |E5| + |E6| + |E7|, \tag{C.6}$$

with

$$E1 = a_h(u_I - u_\pi, d_h), \qquad E2 = \sum_{K\in\mathcal{T}_H} a^K(u_\pi - u, d_h),$$
$$E3 = \int_{\partial\Omega_h} \partial_{\nu_h}(u - \Pi^\nabla(u_I))\widehat{\mathscr{E}}[\Pi^\nabla(d_h)], \qquad E4 = \int_{\partial\Omega_h} \partial_{\nu_h}(u - \Pi^\nabla(u_I))\widehat{\mathscr{C}}\left[\Pi^\nabla(d_h)\right]$$
$$E5 = \int_{\partial\Omega_h} \partial_{\nu_h}(u - \Pi^\nabla(u_I))(d_h - \Pi^\nabla(d_h)), \qquad E6 = \int_{\Omega_h} (f - \Pi^0 f)d_h,$$
$$E7 = \gamma H^{-1}\int_{\partial\Omega_h} (g^\star - \mathscr{E}[\Pi^\nabla(u)])(\gamma H^{-1}\widehat{\mathscr{E}}[\Pi^\nabla(d_h)] - \partial_{\nu_h}\Pi^\nabla(d_h))$$

We observe that we have

$$\|\partial_{\nu_h}\Pi^\nabla(d_h) - \gamma H^{-1}\Pi^\nabla(d_h))\|_{0,\partial\Omega_h} \lesssim H^{-1/2}|||d_h|||_{\Omega_h},$$

as well as

$$\|d_h - \Pi^\nabla(d_h)\|_{0,\partial\Omega_h} \lesssim H^{1/2}|d_h - \Pi^\nabla(d_h)|_{1,\mathcal{T}_H} \lesssim H^{1/2}|||d_h|||_{\Omega_h}.$$

In view of these bound, of (C.1), and of the definition of the norm $|||\cdot|||_{\Omega_h}$, all terms at the right hand side of (C.6) are bound as in [25] and [24], yielding

$$|||u_I - u_h|||_{\Omega_h}^2 \lesssim \left(H^k|u|_{k+1,\Omega} + H^{-1/2}h^{k+1}\|u\|_{k+1,\infty,\Omega}\right)|||u_I - u_h|||_{\Omega_h}.$$

We obtain the desired bound by dividing both sides by $|||u_I - u_h|||_{\Omega_h}$.

References

[1] N. M. Atallah, C. Canuto, G. Scovazzi, The high-order shifted boundary method and its analysis, Computer Methods in Applied Mechanics and Engineering 394 (2022) 114885.

[2] S. Bertoluzza, M. Pennacchio, D. Prada, Weakly imposed Dirichlet boundary conditions for 2d and 3d virtual elements, Computer Methods in Applied Mechanics and Engineering 400 (2022) 115454.

[3] G. Strang, A. E. Berger, The change in solution due to change in domain, in: Partial differential equations, 1973, pp. 199–205.

[4] I. Ramière, Convergence analysis of the q1-finite element method for elliptic problems with non-boundary-fitted meshes, International Journal for Numerical Methods in Engineering 75 (9) (2008) 1007–1052.

[5] N. K. Knowles, J. Kusins, M. P. Columbus, G. S. Athwal, L. M. Ferreira, Experimental DVC validation of heterogeneous micro finite element models applied to subchondral trabecular bone of the humeral head (9) (2022). doi:10.1002/jor.25229.

[6] R. Sun, T. Lei, Q. Chen, Z. Wang, X. Du, W. Zhao, A. K. Nandi, Survey of image edge detection, Frontiers in Signal Processing 2 (2022).

[7] J. Parvizian, A. Düster, E. Rank, Finite cell method, Computational Mechanics 41 (1) (2007) 121–133.

[8] E. Burman, S. Claus, P. Hansbo, M. G. Larson, A. Massing, Cutfem: discretizing geometry and partial differential equations, International Journal for Numerical Methods in Engineering 104 (7) (2015) 472–501.

[9] D. Schillinger, M. Ruess, The finite cell method: A review in the context of higher-order structural analysis of cad and image-based geometric models, Archives of Computational Methods in Engineering 22 (3) (2015) 391–455.

[10] J. H. Bramble, T. Dupont, V. Thomée, Projection methods for Dirichlet's problem in approximating polygonal domains with boundary-value corrections, Math. Comp. 26 (120) (1972) 869–879.

[11] N. M. Atallah, C. Canuto, G. Scovazzi, The shifted boundary method for solid mechanics, International Journal for Numerical Methods in Engineering 122 (20) (2021) 5935–5970.

[12] O. Colomés, A. Main, L. Nouveau, G. Scovazzi, A weighted shifted boundary method for free surface flow problems, Journal of Computational Physics 424 (2021) 109837.

[13] T. Song, A. Main, G. Scovazzi, M. Ricchiuto, The shifted boundary method for hyperbolic systems: Embedded domain computations of linear waves and shallow water flows, Journal of Computational Physics 369 (2018) 45–79.

[14] E. N. Karatzas, G. Stabile, L. Nouveau, G. Scovazzi, G. Rozza, A reduced-order shifted boundary method for parametrized incompressible navier–stokes equations, Computer Methods in Applied Mechanics and Engineering 370 (2020) 113273.

[15] A. Main, G. Scovazzi, The shifted boundary method for embedded domain computations. part I: Poisson and stokes problems, Journal of Computational Physics 372 (2018) 972–995.

[16] N. M. Atallah, C. Canuto, G. Scovazzi, The second-generation shifted boundary method and its numerical analysis, Computer Methods in Applied Mechanics and Engineering 372 (2020) 113341.

[17] E. Burman, P. Hansbo, M. Larson, Dirichlet boundary value correction using lagrange multipliers, BIT Numerical Mathematics 60 (1) (2020) 235–260.

[18] I. Babuška, The finite element method with Lagrangian multipliers, Numer.Math. 20 (1973) 179–192.

[19] R. Stenberg, On some techniques for approximating boundary conditions in the finite element method, Journal of Computational and applied Mathematics 63 (1-3) (1995) 139–148.

[20] E. Burman, P. Hansbo, M. Larson, A cut finite element method with boundary value correction, Mathematics of Computation 87 (310) (2018) 633–657.

[21] J. Cheung, M. Perego, P. Bochev, M. Gunzburger, Optimally accurate higher-order finite element methods for polytopial approximations of domains with smooth boundaries, Mathematics of Computation 88 (319) (2019) 2187–2219.

[22] B. Cockburn, M. Solano, Solving dirichlet boundary-value problems on curved domains by extensions from subdomains, SIAM Journal on Scientific Computing 34 (1) (2012) A497–A519.

[23] Y. Liu, W. Chen, Y. Wang, A weak galerkin mixed finite element method for second order elliptic equations on 2d curved domains, arXiv preprint arXiv:2204.01067 (2022).

[24] S. Bertoluzza, M. Pennacchio, D. Prada, High order VEM on curved domains., Atti Accad. Naz. Lincei Rend. Lincei Mat. Appl. 30 (2019) 391–412.

[25] L. Beirão da Veiga, F. Brezzi, A. Cangiani, G. Manzini, L. D. Marini, A. Russo, Basic principles of virtual element methods, Math. Models Methods Appl. Sci. 23 (1) (2013) 199–214.

[26] L. Beirão da Veiga, F. Brezzi, L. D. Marini, A. Russo, The hitchhiker's guide to the virtual element method, Math. Models Methods Appl. Sci. 24 (8) (2014) 1541–1573.

[27] B. Ahmad, A. Alsaedi, F. Brezzi, L. D. Marini, A. Russo, Equivalent projectors for virtual element methods, Comput. Math. Appl. 66 (3) (2013) 376–391.

[28] L. Beirão da Veiga, F. Dassi, A. Russo, High-order virtual element method on polyhedral meshes, Comput. Math. Appl. 74 (2017) 1110–1122.

[29] L. Beirão da Veiga, F. Brezzi, L. D. Marini, A. Russo, Virtual element method for general second-order elliptic problems on polygonal meshes, Math. Models Methods Appl. Sci. 26 (4) (2016) 729–750.

[30] G. Vacca, L. Beirão da Veiga, Virtual element methods for parabolic problems on polygonal meshes, Numer. Methods Partial Differential Equations 31 (6) (2015) 2110–2134.

[31] L. Beirão da Veiga, C. Lovadina, G. Vacca, Virtual elements for the Navier–Stokes problem on polygonal meshes, SIAM Journal on Numerical Analysis 56 (3) (2018) 1210–1242.

[32] L. Beirão da Veiga, C. Lovadina, G. Vacca, Divergence free virtual elements for the stokes problem on polygonal meshes, ESAIM: M2AN 51 (2) (2017) 509–535.

[33] P. F. Antonietti, L. Beirão da Veiga, D. Mora, M. Verani, A stream virtual element formulation of the Stokes problem on polygonal meshes, SIAM J. Numer. Anal. 52 (1) (2014) 386–404.

[34] L. Beirão da Veiga, C. Lovadina, D. Mora, A virtual element method for elastic and inelastic problems on polytope meshes, Comput. Methods Appl. Mech. Engrg. 295 (2015) 327 – 346.

[35] L. Beirão da Veiga, F. Brezzi, L. D. Marini, Virtual elements for linear elasticity problems, SIAM J. Numer. Anal. 51 (2) (2013) 794–812.

[36] A. L. Gain, C. Talischi, G. H. Paulino, On the virtual element method for three-dimensional linear elasticity problems on arbitrary polyhedral meshes, Comput. Methods Appl. Mech. Engrg. 282 (2014) 132–160.

[37] P. F. Antonietti, L. B. da Veiga, S. Scacchi, M. Verani, A C^1 virtual element method for the Cahn-Hilliard equation with polygonal meshes, SIAM J. Numer. Anal. 54 (1) (2016) 34–56.

[38] I. Perugia, P. Pietra, A. Russo, A plane wave virtual element method for the Helmholtz problem, ESAIM Math. Model. Numer. Anal. 50 (3) (2016) 783–808.

[39] P. Antonietti, S. Bertoluzza, D. Prada, M. Verani, The virtual element method for a minimal surface problem, Calcolo 57 (4) (2020) 39.

[40] M. Frittelli, I. Sgura, Virtual element method for the Laplace-Beltrami equation on surfaces, ESAIM Math. Model. Numer. Anal. 52 (3) (2018) 965 – 993.

[41] D. Mora, G. Rivera, R. Rodríguez, A virtual element method for the Steklov eigenvalue problem, Math. Models Methods Appl. Sci. 25 (8) (2015) 1421–1445.

[42] P. Wriggers, B. Reddy, W. Rust, B. Hudobivnik, Efficient virtual element formulations for compressible and incompressible finite deformations, Computational Mechanics 60 (2) (2017) 253–268.

[43] S. Brenner, L. Sung, Z. Tan, A C^1 virtual element method for an elliptic distributed optimal control problem with pointwise state constraints, Mathematical Models and Methods in Applied Sciences (2021).

[44] L. Beirão da Veiga, F. Brezzi, L. D. Marini, A. Russo, Mixed virtual element methods for general second order elliptic problems on polygonal meshes, ESAIM Math. Model. Numer. Anal. 50 (3) (2016) 727–747.

[45] B. Ayuso de Dios, K. Lipnikov, G. Manzini, The nonconforming virtual element method, ESAIM: Mathematical Modelling and Numerical Analysis 50 (3) (2016) 879–904.

[46] S. Bertoluzza, G. Manzini, M. Pennacchio, D. Prada, Stabilization of the nonconforming virtual element method, Comput. Math. with Appl. 116 (2022) 25–47.

[47] L. Mascotto, I. Perugia, A. Pichler, A nonconforming Trefftz virtual element method for the Helmholtz problem: Numerical aspects, Computer Methods in Applied Mechanics and Engineering 347 (2019) 445–476.

[48] A. Anand, J. S. Ovall, S. E. Reynolds, S. Weißer, Trefftz finite elements on curvilinear polygons, SIAM Journal on Scientific Computing 42 (2) (2020) A1289–A1316.

[49] M. F. Benedetto, S. Berrone, S. Scialó, A globally conforming method for solving flow in discrete fracture networks using the virtual element method, Finite Elem. Anal. Des. 109 (2016) 23 – 36.

[50] L. Beirão da Veiga, C. Lovadina, D. Mora, A virtual element method for elastic and inelastic problems on polytope meshes, Computer Methods in Applied Mechanics and Engineering 295 (2015) 327–346.

[51] H. Chi, L. Beirão da Veiga, G. H. Paulino, Some basic formulations of the virtual element method (vem) for finite deformations, Computer Methods in Applied Mechanics and Engineering 318 (2017) 148–192.

[52] P. Wriggers, W. Rust, B. Reddy, A virtual element method for contact, Computational Mechanics 58 (6) (2016) 1039–1050.

[53] L. Beirão da Veiga, F. Dassi, G. Manzini, L. Mascotto, Virtual elements for Maxwell's equations, Computers & Mathematics with Applications (2021).

[54] J. Nitsche, Über ein variationsprinzip zur Lösung von Dirichlet-Problemen bei Verwendung von Teilräumen, die keinen Randbedingungen unterworfen sind, Abhandlungen aus dem Mathematischen Seminar der Universität Hamburg 36 (1970) 9–15.

[55] L. Beirão da Veiga, C. Lovadina, A. Russo, Stability analysis for the virtual element method, Math. Models Methods Appl. Sci. 27 (13) (2017) 2557–2594.

[56] N. Atallah, C. Canuto, G. Scovazzi, Analysis of the shifted boundary method for the poisson problem in domains with corners, Mathematics of Computation 90 (331) (2021) 2041–2069.

[57] L. Beirão da Veiga, A. Russo, G. Vacca, The virtual element method with curved edges, ESAIM Math. Model. Numer. Anal. 53 (2) (2019) 375–404.

[58] L. Beirão da Veiga, F. Brezzi, L. Marini, A. Russo, Polynomial preserving virtual elements with curved edges, Mathematical Models and Methods in Applied Sciences 30 (08) (2020) 1555–1590.

[59] F. Dassi, A. Fumagalli, D. Losapio, S. Scialò, A. Scotti, G. Vacca, The mixed virtual element method on curved edges in two dimensions, Computer Methods in Applied Mechanics and Engineering 386 (2021) 114098.

[60] F. Aldakheel, B. Hudobivnik, E. Edoardo Artioli, L. Beirão da Veiga, P. Wriggers, Curvilinear virtual elements for contact mechanics, Computer Methods in Applied Mechanics and Engineering 372 (2020) 113394.

[61] F. Dassi, A. Fumagalli, I. Mazzieri, A. Scotti, G. Vacca, A virtual element method for the wave equation on curved edges in two dimensions, Journal of Scientific Computing 90 (1) (2022) 1–25.

[62] E. Artioli, L. Beirão da Veiga, F. Dassi, Curvilinear virtual elements for 2D solid mechanics applications, Computer Methods in Applied Mechanics and Engineering 359 (2020) 112667.

[63] R. Franke, A critical comparison of some methods for interpolation of scattered data, Tech. rep., Naval Postgraduate School Monterey CA (1979).

[64] L. Mascotto, L. Beirão da Veiga, A. Chernov, A. Russo, Exponential convergence of the hp virtual element method with corner singularities, Numer. Math. (2018) 138–581.

[65] P. Jones, Quasiconformal mappings and extendability of functions in Sobolev spaces, Acta Math. 147 (1981) 71–88.